Department of Physics and Astronomy
University of Heidelberg

Bachelor Thesis in Physics
submitted by

Florian Haslbeck

born in Fulda (Germany)

2019

Saturation Studies for the Modified Analog Signal Path in the ATLAS Level-1 Calorimeter Trigger Phase-I Upgrade

This Bachelor Thesis has been carried out by Florian Haslbeck at the
Kirchhoff-Institute for Physics in Heidelberg
under the supervision of
Prof. Dr. Hans-Christian Schultz-Coulon.

Abstract

The new Trigger Digitiser Boards of the LAr calorimeter which are installed during the Phase-I Upgrade will deliver higher granularity and longitudinal shower information to the ATLAS Level-1 Calorimeter Trigger in Run 3. The Run 2 trigger tower based legacy trigger system is kept operational by feeding the new signals to the Tower Builder Board via a new analog signal path.

In this thesis the linearity of the Run 2 digitisation system before and after the Phase-I upgrade is compared. Run 2 calibration pulser runs are characterised regarding the linearity of trigger towers to provide a reference for commissioning of the new electronics.

Two iterative linear fit methods are developed in which cuts on the residual or the chi squared reduced are applied. The residual method is found to be more stable.

So far, one LAr Trigger Digitiser Board is installed. The Level-1 Calorimeter Trigger input signals have not been synchronised and are thus delayed by six to ten nanoseconds with respect to the Run 2 system. Therefore, the signal is digitised earlier and the characterisation of the digitised signal can only be partially compared to the Run 2 system.

Zusammenfassung

Während des Phase-I Upgrades werden neue Trigger Digitiser Boards für die LAr Kalorimeter installiert, damit der ATLAS Level-1 Calorimeter Trigger in Run 3 mit erhöhter und longitudinalen Shower Kalorimeter Auflösung betrieben werden kann. Das Trigger Tower basierte Run 2 System wird weiterhin betrieben, das neue analoge Signal wird daher den Tower Builder Boards mittels eines neuen Signalweges übergeben.

Die Linearität der Run 2 Signal Digitalisierung wird vor und nach dem Upgrade charakterisiert. Die Run 2 Trigger Kalibrationsruns werden, unterteilt in Trigger Tower, bezüglich der Linearität untersucht und als Referenz für das Phase-I Upgrade bereitgestellt.

Zwei iterative lineare Fitmethoden basierend auf Grenzwerten für das Residuum oder das reduzierte Chi-Quadrat wurden entwickelt. Die residuenbasierte Methode funktioniert zuverlässiger.

Bisher wurde ein LAr Trigger Digitiser Board installiert. In Folge des noch nicht synchronisierten veränderten Kalorimetersignalweges erfolgt die Digitalisierung verzögert, sodass die Lineritätscharaktersierung nur eingeschränkt mit den Run 2 Ergebnissen vergleichbar ist.

Contents

1. Introduction **1**
- 1.1. Large Hadron Collider . . . 1
- 1.2. ATLAS Detector . . . 2
- 1.3. ATLAS Level-1 Calorimeter Trigger . . . 4
- 1.4. Phase-I Upgrade . . . 8

2. Level-1 Calorimeter Trigger Saturation Studies **10**
- 2.1. Trigger Tower Linearity Characterisation . . . 10
  - 2.1.1. Level-1 Calorimeter Trigger Pulser Runs . . . 10
  - 2.1.2. Trigger Tower Linearity Characterisation Method . . . 12
- 2.2. Residual Threshold Algorithm . . . 15
- 2.3. Chi Squared Reduced Threshold Algorithm . . . 15
- 2.4. Threshold Determination . . . 16
  - 2.4.1. Residual Threshold Determination . . . 16
  - 2.4.2. Chi Squared Reduced Threshold Determination . . . 19

3. Results **21**
- 3.1. Time Slice n . . . 22
- 3.2. Time Slice n-1 . . . 26
- 3.3. Time Slice n-2 . . . 28

4. Conclusion **32**

Appendix **33**
- A. Threshold Determination . . . 33
  - A.1. Residual Threshold Determination . . . 33
  - A.2. Chi Squared Reduced Threshold Determination . . . 35
- B. Results . . . 37
  - B.1. Time Slice n . . . 37
  - B.2. Time Slice n-1 . . . 38
  - B.3. Time Slice n-2 . . . 40
  - B.4. Time Slices n-0.5, n-1.5 . . . 42

1. Introduction

After three years of data taking, the Large Hadron Collider's (LHC) second run, Run 2, ended on 3 December 2018 [5]. The full dataset allows an even more sophisticated analysis of the Higgs boson, which was already discovered with data from Run 1 [9]. The mass measurement of the Higgs boson, top quark and W boson are increased to a new level of precision. Not only the statistical uncertainties can be reduced using the full integrated luminosity of the Run 2 dataset, but also new, sophisticated algorithms are developed to further reduce the systematic uncertainties.

During the upcoming second long shutdown, the LHC will be upgraded to its design center-of-mass energy. Therefore, the pre-accelerators and experiments will also be modified for an enhanced physics search before the LHC will return taking data during Run 3 starting in 2021.

This thesis studies the saturation behaviour for the modified analog signal path for the ATLAS Level-1 Calorimeter Trigger during the Phase-I Upgrade.

The LHC and the ATLAS (A Toroidal LHC Apparatus) experiment are briefly outlined in the first chapter with special regards to the ATLAS calorimeter and the Phase-I Upgrade of the Level-1 Calorimeter Trigger. The algorithms developed for the saturation characterisation are described in Chapter 2, followed by the results in Chapter 3. A conclusion is given in Chapter 4.

1.1. Large Hadron Collider

The LHC [2] at CERN is the world's most powerful circular particle collider. The proton[1] accelerator chain begins with a linear accelerator (LINAC), followed by the Proton Synchrotron Booster, the Proton Synchrotron and the Super Proton Synchrotron before the protons are inserted into the LHC ring. Inside the two LHC beam pipes the protons circulate in opposite directions before they collide at the four interaction points (IPs). There, the four large LHC experiments are placed: ATLAS, CMS (Compact Muon Solenoid), ALICE (A Large Ion Collider Experiment) and LHCb (Large Hadron Collider beauty).

The general-purpose detectors ATLAS and CMS study a shared broad range of physics, for example Standard Model processes, extra dimensions or dark matter, both using their own approach in order to verify each others results.

[1] Usually, the LHC is operated with proton – proton collisions but also heavy ions can be collided using a different pre-accelerator chain.

ALICE studies heavy ion collisions in order to understand quark-gluon-plasmas which could have existed shortly after the Big Bang.

LHCb investigates CP-violations with 'beauty quarks' to study the asymmetry between matter and antimatter.

The LHC beam is divided into maximal 2808 bunches time wise separated by 25 ns. In Run 2 (2015 – 2018) [3], each bunch was filled with up to 10^{11} protons. During Run 2 the LHC had a center-of-mass energy of $\sqrt{s} = 13\,\text{TeV}$ and the luminosity reached up to $\mathcal{L} \approx 2 \times 10^{34}\,\text{cm}^{-2}\text{s}^{-1}$. In Run 3, starting in 2021, the LHC will be run with an increased center-of-mass energy of $\sqrt{s} = 14\,\text{TeV}$ and a luminosity of $\mathcal{L} \approx 2.3 \times 10^{34}\,\text{cm}^{-2}\text{s}^{-1}$ [1]. To achieve this performance and enhance the physics studies, the accelerators and experiments are upgraded during the second long LHC shutdown.

1.2. ATLAS Detector

The ATLAS experiment [4] is a general-purpose particle detector. The 25 m wide and 44 m long detector is shown in Figure 1.1. It features a forward-backward symmetry with respect to the nominal IP in the center and covers an area of almost 4π in the solid angle. The determination of the energy, momentum and location of a particle is based on several subsystems which are outlined in the following.

ATLAS uses a right-handed coordinate system with the origin situated in the nominal IP. The z-axis points along the beam pipe, the x-axis points from the IP to the center of the LHC ring and the y-axis is directed upwards. Further, the cylindrical coordinates (r, ϕ, η) are used in the transverse plane with respect to the beam pipe with the azimuthal angle ϕ around the z-axis and the polar angle θ. The pseudorapidity η is then defined as $\eta = -ln\tan(\theta/2)$ and the transverse energy with $E_\text{T} = E/\cosh(\eta)$.

Immersed in the 2 T magnetic field generated by the central solenoid, the *inner tracking detector* (ID) provides reconstructed tracks from primary proton – proton collisions and identifies the tracks of secondary vertices. This enables a pile-up handling by distinguishing the background processes from the collisions of interest per LHC bunch-crossing (BC). The magnetic field bends the tracks of particles with electric charges. The particles' charges and momenta are determined by the three ID sub-detectors:

The high granularity silicon pixel detector is placed closest to the IP. It is enclosed by the pixel strip detector. Both sub-detectors cover $|\eta| < 2.5$. The pixel sub-detectors are surrounded by the transition radiation tracker covering $|\eta| < 2.0$ which detects photon transition radiation and hereby provides particle identification.

The ATLAS calorimetry is divided into the electromagnetic (EM) calorimeter which is enclosed by hadronic (HAD) calorimeter, as it is depicted in Figure 1.2. The ATLAS calorimeter covers $|\eta| < 4.9$ and is adapted spatial wise to different detector characteristics, for example by optimising the absorber thickness to the η dependent energy resolution. Most electrons (positrons) and photons deposit their energy by electromag-

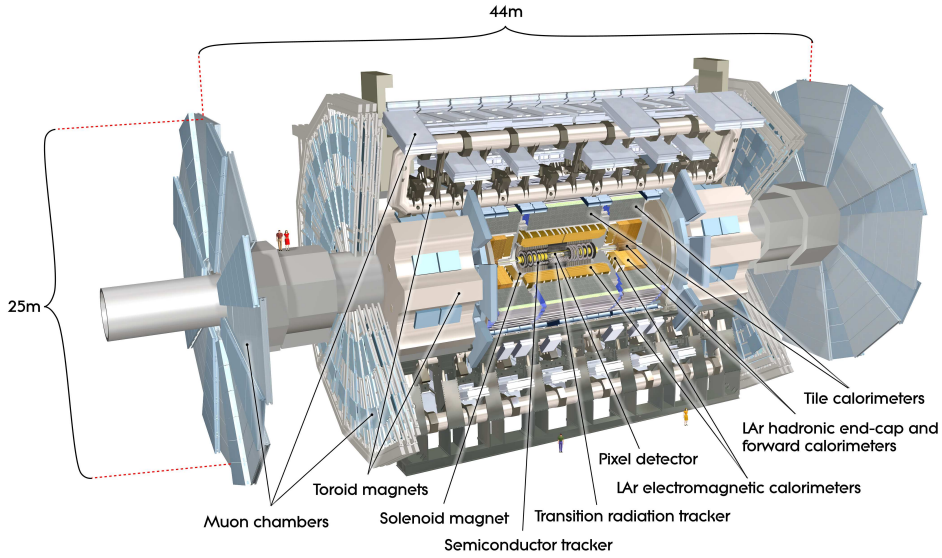

Figure 1.1.: Cutaway view of the ATLAS detector [4].

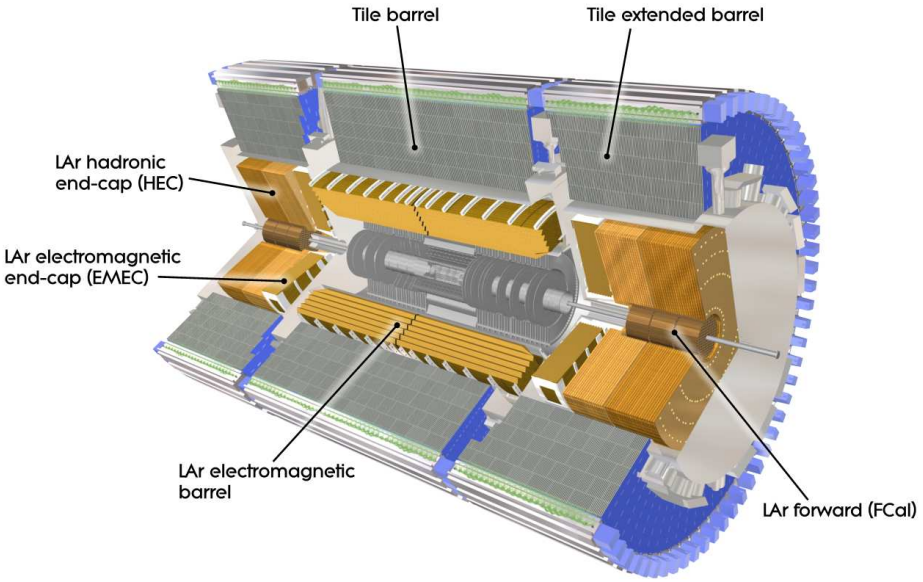

Figure 1.2.: Cutaway view of the ATLAS calorimeter system [4].

EMB			$\lvert\eta\rvert$	$<$	1.475
EMEC outer wheel	1.375	$<$	$\lvert\eta\rvert$	$<$	2.5
EMEC inner wheel	2.5	$<$	$\lvert\eta\rvert$	$<$	3.2
FCal	3.1	$<$	$\lvert\eta\rvert$	$<$	4.9

Table 1.1.: η coverage for the electromagnetic calorimeter components [4].

netic showering in the EM calorimeter. Hadrons deposit only a fraction of their energy in the EM calorimeter because of their larger radiation length. Therefore, the HAD calorimeter contains more absorber material in order to measure the hadrons energy.

The EM calorimeter is a lead/liquid argon (LAr) sampling calorimeter. The particles shower in the lead absorbers and ionise the liquid argon. The accordion-shaped calorimeter cells ensure a symmetric ϕ coverage. The EM calorimeter is divided into a central barrel (EMB), two end-caps (EMEC), which are sub-divided into the EMEC outer wheel and the EMEC inner wheel, and the forward calorimeter (FCal). The η coverage for the electromagnetic calorimeter components is given in Table 1.1. A pre-sampler is used for $|\eta| < 1.8$ to correct for electron and photon upstream of the calorimeter.

The HAD calorimeter consists of a tile barrel calorimeter covering $|\eta| < 1.7$ using tile scintillators as active and steel for the passive components. The HAD end-caps are copper/LAr sampling calorimeters and cover $1.5 < |\eta| < 3.2$. The two hadronic forward calorimeters use copper/LAr and tungsten/LAr for passive/active components. The HAD forward calorimeter covers up to $|\eta| < 4.9$.

Because of the small muon interaction cross section in the detector, the muon detector is the outermost ATLAS sub-detector. The muon detector is divided in precision tracking and calorimetry and is immersed in a second magnetic field which is inversely orientated to the inner magnetic field.

1.3. ATLAS Level-1 Calorimeter Trigger

The enormous amount of data given by a collision frequency of 40 MHz and an average number of interactions per bunch-crossing of $< \mu >= 33.7$ (Run 2) [3] requires a trigger system to select events for permanent storage. The ATLAS three-level trigger system [6], [8] consists of a custom hardware-based first-level (L1) trigger, a software-based second-level trigger and an event filter. It triggers events containing processes of interest.

Based on reduced granularity detector data, the L1 trigger suppresses the event acceptance rate to a maximum of 100 kHz. If the L1 issues a L1 trigger accept (L1A) signal, the data acquisition system read out the detector for the selected event and forwards it to the high-level trigger. After the event filter, the data is permanently stored with a maximum average rate of 1 kHz.

The L1 trigger decision is formed by three sub-trigger systems: the L1 Calorimeter (L1Calo) trigger, the L1 Muon trigger and the L1 Topological trigger. The L1Calo and

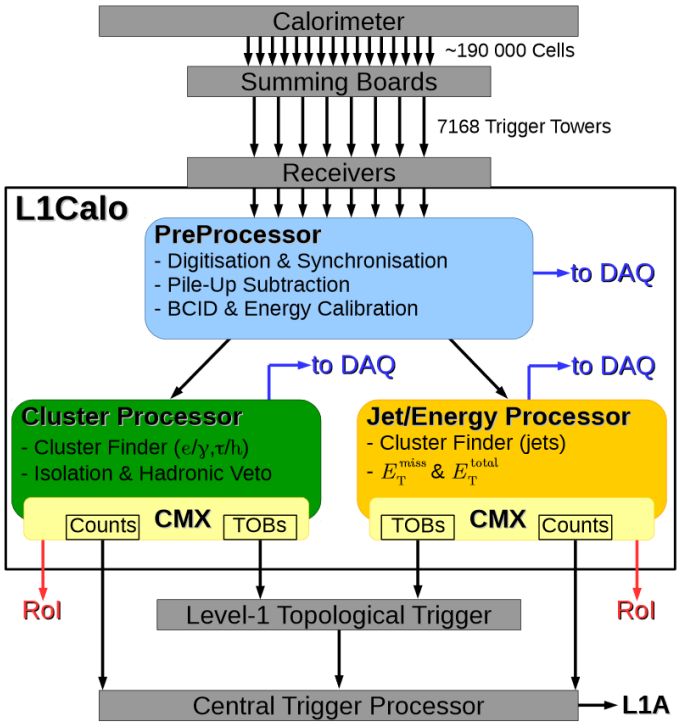

Figure 1.3.: Architecture of the L1Calo trigger in Run 2 [8].

L1 Muon trigger identify physics objects candidates per event in the corresponding sub-detector which contain high-E_T particles. For those events, the L1 Topological trigger analyses the event topology. All three trigger results are collected by the Central Trigger Processor which forms eventually the L1A decision.

A scheme of the Run 2 L1Calo trigger is given Figure 1.3. The detector front-end buffers limit the L1 trigger decision time to 2.5 μs out of which only about 1 μs can be used for processing due to the signal transmission time. The PreProcessor (PPr) prepares the calorimeter signals by digitising, synchronising and calibrating them to the correct transverse energy. Further, the pile-up is subtracted and the LHC bunch-crossing with the highest E_T identified (BCID). Electron, photon and tau candidates are identified by the Cluster Processor, jet candidates are handled by the Jet/Energy Processor which further computes global energy sums like the missing or the total energy. The Common Merger Modules (CMX) collect the identified candidates and transmit them as Trigger Objects (TOBs) to the L1 Topological trigger. For a L1A signal, all L1Calo data is read out by the Data Acquisition System (DAQ). This allows the reconstruction of the trigger decision and performance. In addition, Regions-of-Interest (RoI) are thereby formed and are forwarded to the high-level trigger.

The L1Calo trigger receives reduced calorimeter data in terms of 7168 projective trigger towers (TTs) divided in 66 η and 64 ϕ stripes. In the following, the electromagnetic TT forming is outlined. The calorimeter cell signals are summed up for the three

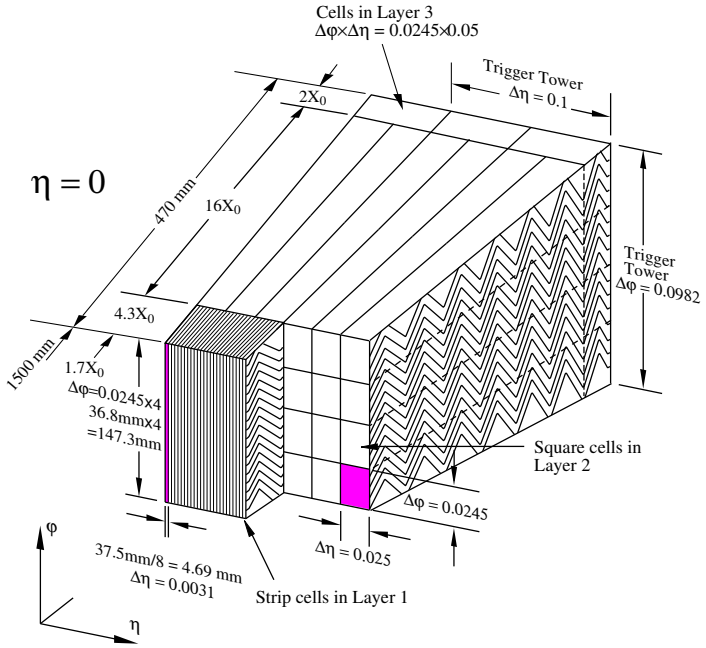

Figure 1.4.: EMB TT consisting of accordion-shaped calorimeter cells [4].

calorimeter layers and grouped in defined $\eta - \phi$ regions by the Trigger Tower Builder boards. A EMB TT has a size of $(\Delta\eta \times \Delta\phi) = (0.1 \times 0.1)$ and sums the cells in layer 1, 2 and 3, shown in Figure 1.4. EMEC TTs sum up a large region (0.2×0.2), in the FCal it extends to (0.4×0.4). The TT granularity for EMB, EMEC and FCal is demonstrated in Figure 1.5.

The TT signals are fed to the L1Calo trigger via receiver boards and are routed to the PreProcessor (PPr) receiver modules. They compensate for signal attenuation and calibrate the signals to a common energy scale by providing variable gain. The calibrated signal shape for the EMB and the EM FCal are given in Figure 1.6. Further, the trigger signals are synchronised, digitised and assigned to correct LHC BC. One analog-

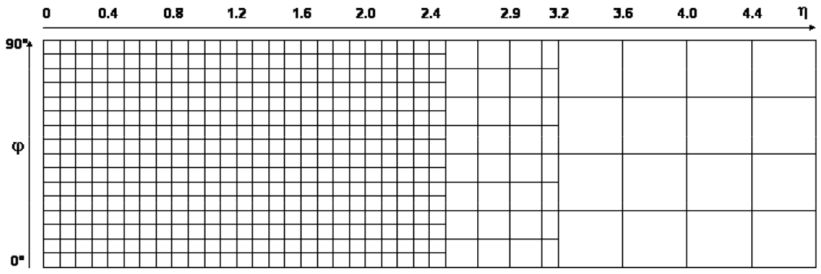

Figure 1.5.: TT granularity in the EM calorimeter for $\eta > 0$ and the first quadrant in ϕ. The layout for the other quadrants is identical and mirrored for $\eta < 0$ [6].

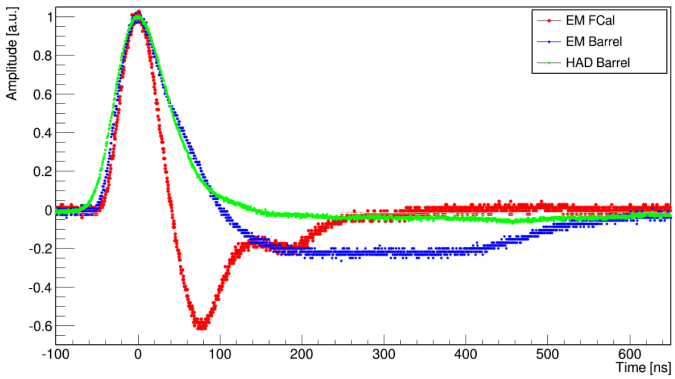

Figure 1.6.: Normalised pulse shapes for trigger towers in the EMB – blue, EM FCal – red and the hadronic barrel – green. The signals are recorded with an oscilloscope during proton-proton collisions at the receiver output [8].

to-digital converter (ADC) count in the signal height corresponds to a $E_{\mathrm{T}}^{\mathrm{Calo}}$ deposition of $\approx 0.25\,\mathrm{GeV}$. A digital offset of 32 ADC counts is chosen to account for the signals' undershoot, which are seen for the EM FCal and EMB in Figure 1.6.

The BCID [10] is the central task of the PPr. It is very important, because the detector is only readout by the L1 trigger for the correctly identified BC. A misidentified BC results in partially lost event information. Furthermore, the high-level trigger would then operate on wrong event information and falsely reject the event. Depending on the signals saturation, two distinct methods are performed: a peak finder optimised for low-E_{T} non-saturated signals and a threshold-based algorithm for pulses which saturate the analog-to-digital converter.

The peak finder removes pile-up contributions and applies a peak condition to identify the bunch crossing containing the highest-E_T particles. TT signals with more than 250 GeV ($E_{\mathrm{T}}^{\mathrm{Calo}}$) saturate the ADC at 1023 ADC counts. For transverse energies above 250 GeV, multiple ADC samples can saturate, therefore, the standard peak condition is unable to identify the correct LHC BC. The saturated BC identification algorithm compares the two non-saturated ADC samples before saturation on the rising pulse edge with chosen thresholds and identifies the BC corresponding to the peak of the saturated signal. The algorithm extrapolates linearly the non-saturated part of the pulses to the saturated regime. It is crucial to study the performance of the saturated-pulse algorithms in the context of the Phase-I Upgrade, which is described in the following Section.. Therefore, this thesis performs saturation studies for the modified analog signal path for the Phase-I upgrade and characterises the trigger tower linearity for saturated pulses.

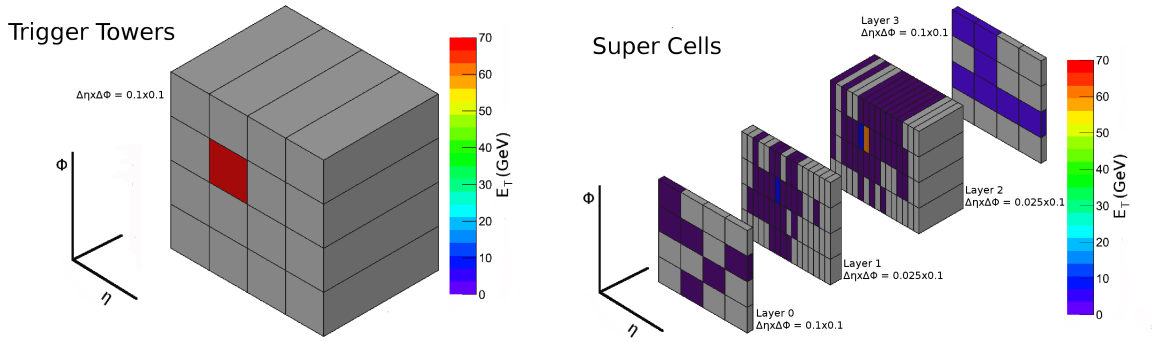

(a) (b)

Figure 1.7.: An electron with $E_{\mathrm{T}} = 70\,\mathrm{GeV}$ as seen by the existing L1 Calo trigger electronics (a) and by the upgraded trigger electronics (b) [1].

1.4. Phase-I Upgrade

During the Phase-I Upgrade [1] new L1 Calorimeter trigger electronics will be installed. Higher resolution, higher granularity in η and longitudinal shower information will be delivered from the calorimeters to the L1 trigger. The trigger energy resolution and selection efficiency for electrons, photons, taus, jets and missing transverse energy is improved. Furthermore, the background and fake discrimination for example for pile-up is enhanced, which allows the ATLAS detector to exploit the luminosity increase up to $\mathcal{L} \approx 2.2 \times 10^{34}\mathrm{cm}^{-2}s^{-1}$, an expected bunch crossing spacing of 25 ns and an average number of interactions per crossing of $< \mu > \approx 60$ for Run 3. The Phase-I Upgrade is designed with some margin for a maximal luminosity of $\mathcal{L} = 3 \times 10^{34}\mathrm{cm}^{-2}s^{-1}$ and a maximal average number of interactions pre event of $< \mu > \approx 80$.

The upgraded trigger system is based on 'super cells'. The calorimeter cells are clustered with a finer segmentation of $(\Delta\eta \times \Delta\phi) = (0.025 \times 0.1)$ in the front and middle layers for the EMB amd EMEC for $|\eta| < 2.5$. The pre-sampler and back layer are kept within clusters of $(\Delta\eta \times \Delta\phi) = (\Delta 0.1 \times 0.1)$. Figure 1.7 visualises the signal of an electron with $E_T = 70\,\mathrm{GeV}$ in the electronics as used in Run 2, Figure 1.7a and in the the upgraded electronics, Figure 1.7b. In Run 2, a prototype of the new system was successfully tested in the EMB. The upgraded L1Calo trigger electronics is outlined in Figure 1.8.

Furthermore, the LAr Trigger Digitiser Board (LTDB) recreates the Run 2 granularity $(\Delta\eta \times \Delta\phi) = (\Delta 0.1 \times 0.1)$ and feeds them to the Tower Builder Board (TBB). Hereby, the Run 2 legacy system is kept operational. This thesis studies the saturation behaviour for the modified analog signal path to the TBB as indicated as red thick lines in Figure 1.8.

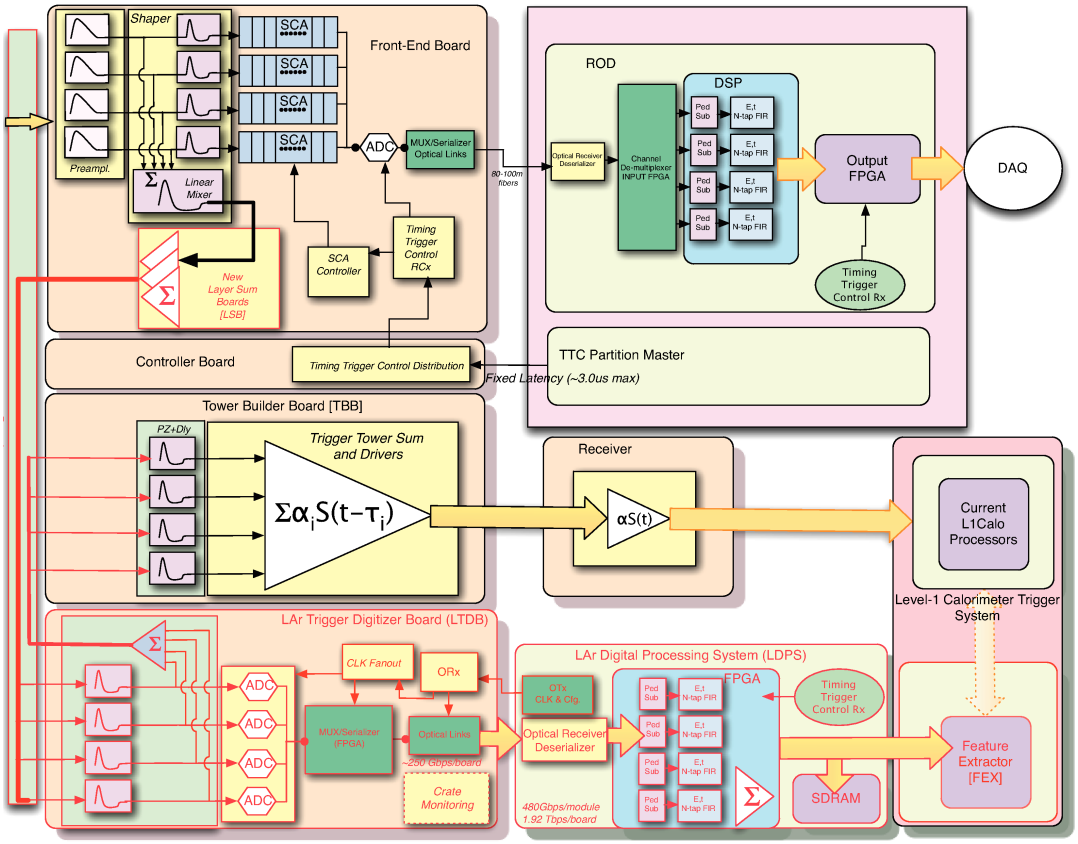

Figure 1.8.: Schematic block diagram of the Phase-I upgrade LAr trigger readout architecture. The new components are indicated by the red outlines. The yellow arrow on the upper left indicates the calorimeter input [1].

2. Level-1 Calorimeter Trigger Saturation Studies

This chapter covers the methodology of the Level-1 Calorimeter trigger saturation studies. Section 2.1 describes the trigger tower characterisation by outlining the LAr calorimeter pulser runs in Subsection 2.1.1 and explaining the trigger tower linearity characterisation in Subsection 2.1.2. The two iterative fit routines, the residual threshold algorithm and the χ^2_{red} threshold algorithm are outlined in Section 2.2 and Section 2.3, respectively.

2.1. Trigger Tower Linearity Characterisation

The saturation studies check the Run 2 Level-1 Calorimeter (L1Calo) trigger electronics before and after the Phase-I Upgrade. Calibration pulser runs are characterised regarding the linearity of trigger towers to provide a reference for commissioning of the new electronics. Pulser runs for the Run 2 trigger system with a digitisation frequency of 40 MHz are used to develop the linearity characterisation method and to provide a reference for the commissioning. At the time of this thesis, only one LAr Trigger Digitiser Board (LTDB) has been installed. The new LTDB is analysed and compared to the corresponding Run 2 system data. Once the Phase-I Upgrade is completed, commissioning data for Run 3 can be taken and analysed.

2.1.1. Level-1 Calorimeter Trigger Pulser Runs

Pulser Runs and Time Slice Naming Convention

A calibration system is used to check the L1Calo trigger electronics. Discrete electric charges are injected in the front-end boards of the electromagnetic calorimeter. For a given charge injection, all calorimeter cells are pulsed and read out using the same electronics path as physics signals, hence each injection generates one event. A ramp with steps of increasing energy is referred to as a *pulser run*. Usually, 200 charge injections are done per energy step.

Figure 2.1 shows a sketch of a pulser run signal digitisation after pulse shaping and the corresponding time slice naming convention. The analog-to-digital converter (ADC) counts are referred to as *sample height*. The 40 MHz digitisation frequency is depicted in Figure 2.1a, the 80 MHz digitisation frequency in Figure 2.1b. The signal rise time of 50 ns is determined by the LAr calorimeter electronics. The falling edge is given by a

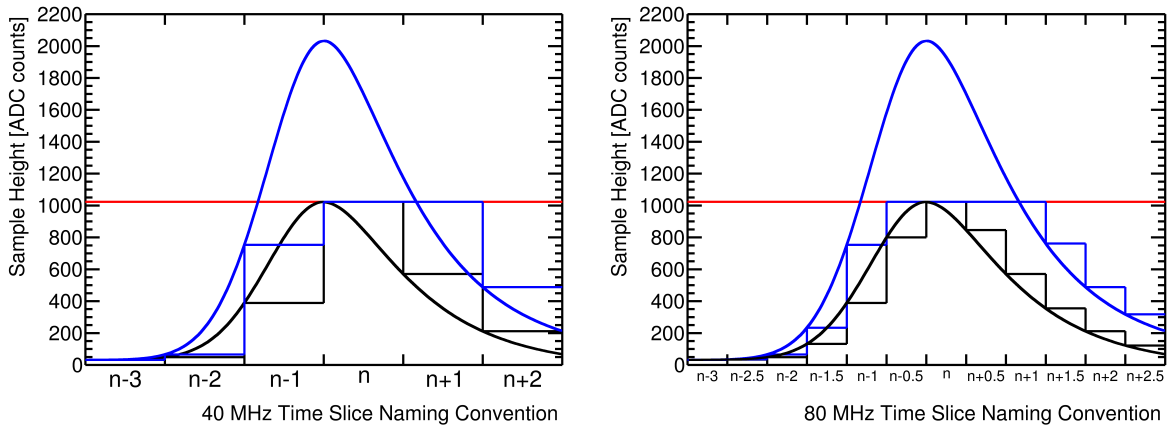

(a) 40 MHz pulser run signal digitisation and time slice naming convention.

(b) 80 MHz pulser run signal digitisation and time slice naming convention.

Figure 2.1.: Pulser run signal digitisation after shaping and time slice naming convention for 40 MHz and 80 MHz digitisation frequency. A high charge injection signal is digitised, shown in blue. The maximal ADC count of 1023 ADC counts is shown in red. The digitisation of a lower charge injection signal is shown in black.

Landau distribution with a amplitude dependent falling time. The analog pedestal has a digitised sample height of 32 ADC counts. The time slice naming convention declares the slice containing the signal's peak with 'n'. For a 40 MHz digitisation frequency, each time slice is 25 ns wide and an integer naming convention is chosen, depicted in Figure 2.1a. Given the rise time of 50 ns, the pulse is injected in time slice n-2. The 80 MHz digitisation frequency increases the time resolution to a 12.5 ns slice width, which is considered in the half-integer naming convention, Figure 2.1b. Still, the pulse is injected in time slice n-2, the digitised peak is stored in slice n.

Figure 2.2 shows the pulser runs for the trigger tower (TT), $\eta = 2.0$, $\phi = 1.2$ before and after the Phase-I Upgrade. At time slice n the saturation at ≈ 250 GeV is seen in red for both digitisation frequencies. At slice n-1 (green) the signal does not saturate until a charge injection corresponding to an $E_{\mathrm{T}}^{\mathrm{Calo}}$ energy of ≈ 400 GeV for the Run 2 system and ≈ 600 GeV for the upgraded system. In time slice n-2 (blue) the signal does not saturate.

Pulser Run Data Handling

During a pulser run a discrete charge is injected usually 200 times into all calorimeter front-end boards [10]. All shaped signals are read out for all calorimeter cells. This analysis clusters all 200 injections in one *point*. In the case that the last injection step consists of less than 200 events, the injections are still grouped as a last data point.

The $E_{\mathrm{T}}^{\mathrm{Calo}}$ is read out with a precision of 1 GeV and the sample height with 1 ADC

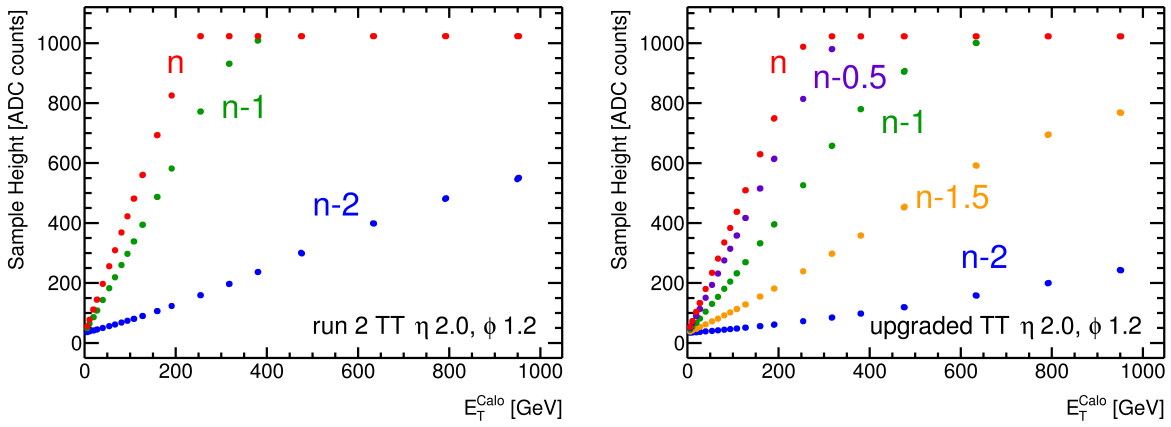

(a) Run 2 TT with 40 MHz digitisation frequency.

(b) Phase-I upgraded TT with 80 MHz digitisation frequency.

Figure 2.2.: Pulser run time slices for the TT at $\eta = 2.0$, $\phi = 1.2$. (a) shows the Run 2 TT with at 40 MHz digitisation frequency, (b) depicts the upgraded TT with a 80 MHz digitisation frequency.

count. For a point, the measured $E_{\mathrm{T}}^{\mathrm{Calo}}$ deviate by ± 2 GeV and ± 5 ADC counts. For each $E_{\mathrm{T}}^{\mathrm{Calo}}$ bin, the mean sample height with the standard error on the mean is stored. For non-empty bins with N entries and a standard deviation of zero, the standard deviation of $1/\sqrt{12\ N}$ is used. This takes the uncertainty of one half ADC count into account. The uncertainty in $E_{\mathrm{T}}^{\mathrm{Calo}}$ is given by 0.5 GeV determined by the binning [7].

The fit, see Subsection 2.1.2, takes each filled bin with the corresponding error into account. To ensure that every injection per chosen charge is taken into account, the fit range is extended point per point. For each point, the weighted mean *sample height* $\overline{Point}$ and $E_{T\,\overline{Point}}^{Calo}$ are calculated.

2.1.2. Trigger Tower Linearity Characterisation Method

The L1Calo trigger saturation studies aim for an understanding of the saturation behaviour for the trigger electronics in terms of TTs. Therefore, the last linear point (LLP) of the pulser run is identified for each TT. If the pulser run contains more points, the next point is declared as the first non-linear point (NLP).

Sections 2.2 and 2.3 give a more detailed description of the algorithms used for the non-linearity studies. This Subsection outlines the general method and its performance criteria.

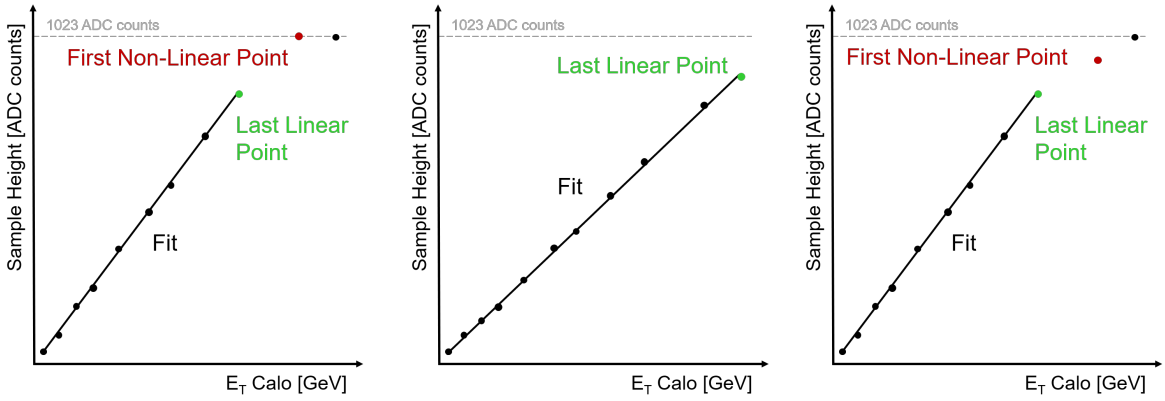

(a) Linear until saturation. (b) Linear and not saturated. (c) Not linear.

Figure 2.3.: Overview of the three trigger tower linearity categories.

Iterative Fit Approach

The linearity characterisation relies on an iterative fit range approach. A linear function with two free parameters, the slope and the ordinate, Equation (2.1), is fitted with no restrictions on either of the both parameters.

$$\text{linear fit} := \text{slope} \times E_T^{Calo} + \text{ordinate}. \tag{2.1}$$

The iteration starts fitting the first four points of the pulser run. The restriction to four points improves the fit stability and ensures that the variation at low injection energies and sample heights are not misidentified as a non linearity. The fit range is iteratively extended point per point and every single $E_{\mathrm{T}}^{\mathrm{Calo}}$ bin is considered with the assigned error, as described in Subsection 2.1.1. Applying cuts on the sample height $\overline{\text{Point}}$ or on the χ^2_{red} , the methods identify the last linear point and store the parameters of the last linear fit. If the pulser run contains more points, the first non-linear point is declared, too.

Trigger Tower Linearity Characterisation

The methods characterise a trigger tower (TT) within three categories, *linear until saturation*, *linear and not saturated* and *not linear*, which are sketched in Figure 2.3.

A TT is declared as *linear until saturation*, if the first non-linear point sample height $\overline{\text{Point}}$ is equal to or greater than 1020 ADC counts, Figure 2.3a. Defining the saturation at 1020 instead of 1023 ADC counts considers the case of a saturated point which is slightly scattered in the measured $E_{\mathrm{T}}^{\mathrm{Calo}}$ and/ or sample height.

If the algorithm finds the last linear point equal to the last data point, the TT is declared as *linear and not saturated*, Figure 2.3b and no first non-linear point is identified.

If none of the previous cases is found, the TT is declared as *not linear*, shown in Figure 2.3c.

Residual and E_T^{Calo} Deviation

The TT linearity characterisation performance is controlled with the residual and the deviation in $E_{\mathrm{T}}^{\mathrm{Calo}}$ for the last linear and the first non-linear point. Furthermore, the residual threshold algorithm, described in Section 2.2, applies a residual cut for the linearity characterisation. The residual and $E_{\mathrm{T}}^{\mathrm{Calo}}$ deviation calculation uses the last linear fit parameters (slope $_{\mathrm{Fit}}$ and ordinate $_{\mathrm{Fit}}$) and the deviation with respect to the corresponding mean sample height $_{\overline{\mathrm{Point}}}$ and $E_{\mathrm{T}\,\overline{\mathrm{Point}}}^{\mathrm{Calo}}$.

The *residual* is defined as the sample height difference between the last linear fit and the corresponding point. It is calculated by evaluating the fit at the mean $E_{\mathrm{T}\,\overline{\mathrm{Point}}}^{\mathrm{Calo}}$ of the corresponding point minus its mean sample height $_{\overline{\mathrm{Point}}}$, see Equation (2.2) or Figure 2.4.

$$\text{residual} = (\text{slope}_{\,\mathrm{Fit}} \times E_{\mathrm{T}\,\overline{\mathrm{Point}}}^{\mathrm{Calo}} + \text{ordinate}_{\,\mathrm{Fit}}) - \text{sample height}_{\,\overline{\mathrm{Point}}}. \tag{2.2}$$

The E_T^{Calo} *deviation* is defined as the $E_{\mathrm{T}}^{\mathrm{Calo}}$ difference between the fit and the $E_{\mathrm{T}\,\overline{\mathrm{Point}}}^{\mathrm{Calo}}$ see Equation (2.3). It is calculated by the mean $E_{\mathrm{T}\,\overline{\mathrm{Point}}}^{\mathrm{Calo}}$ value minus the difference of the mean sample height $_{\overline{\mathrm{Point}}}$ and the fit's ordinate divided by the slope.

$$E_T^{Calo}\,\text{deviation} = E_{\mathrm{T}\,\overline{\mathrm{Point}}}^{\mathrm{Calo}} - \frac{\text{sample height}_{\overline{\mathrm{Point}}} - \text{ordinate}_{\,\mathrm{Fit}}}{\text{slope}_{\,\mathrm{Fit}}}. \tag{2.3}$$

The residual and the $E_{\mathrm{T}}^{\mathrm{Calo}}$ deviation are defined as such, that a saturated and therefore non linear point has a positive residual and a positive $E_{\mathrm{T}}^{\mathrm{Calo}}$ deviation, as it is shown at the last point taken into account by the fit, Figure 2.4.

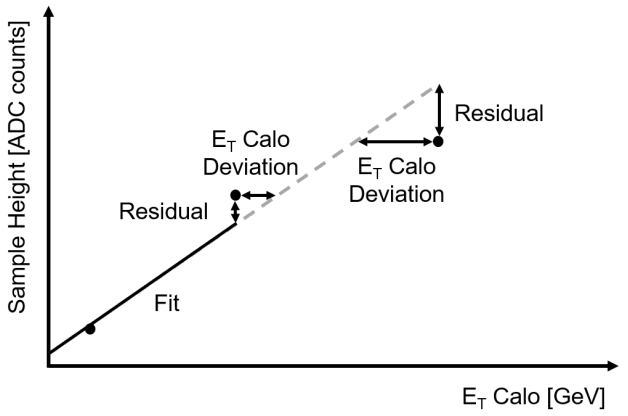

Figure 2.4.: Residual and the $E_{\mathrm{T}}^{\mathrm{Calo}}$ deviation calculation for the last point included and the first point not included in the fit range. The fit is shown as a black solid line, the extrapolation as a grey dashed line.

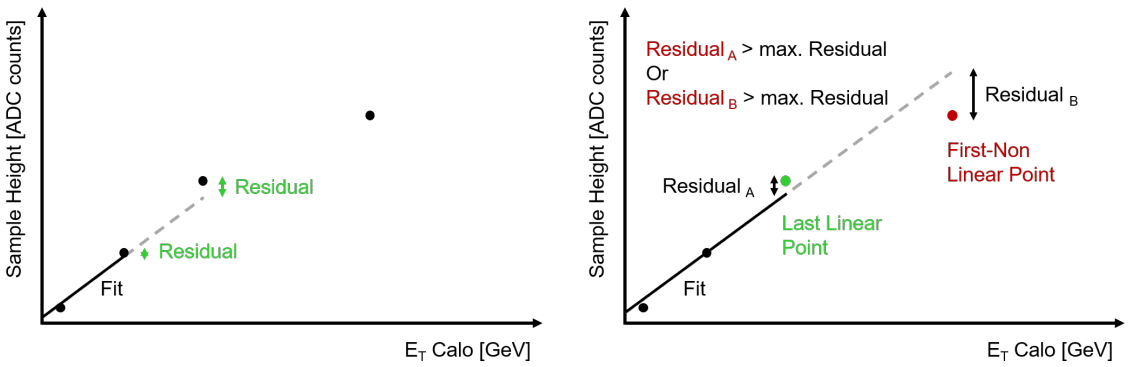

(a) Residual calculation for the last point included in the fit range and the first point not included in the fit range.

(b) The residual for the next point exceeds the resiudal threshold and the LLP and the NLP are identified.

Figure 2.5.: The residual threshold algorithm. The fit is shown as a black solid line, the extrapolation as a grey dashed line.

2.2. Residual Threshold Algorithm

The residual threshold algorithm extends the fit range iteratively point by point. As it is shown in Figure 2.5a, the residuals are calculated for the last point included in the fit range and for the first point which is not included in the fit range by extrapolating the fit. If one of the residuals exceeds a predefined threshold, the routine stops. The last point included in the fit range is then defined as the last linear point, the next point defined as the first non-linear point, Figure 2.5b.

The residual threshold algorithm characterises the TT linearity accordingly to Subsection 2.1.2. If the first non-linear point mean sample height $\overline{\text{Point}}$ is equal to or greater than 1020 ADC counts, the TT is declared *linear till saturation*. If the last linear point is also the last data point the TT is declared as *linear and not saturated*. Else, the TT is characterised *not linear*.

2.3. Chi Squared Reduced Threshold Algorithm

The χ^2_{red} threshold algorithm extends the fit range iteratively point by point and compares the χ^2_{red} values with respect to the fit before. The method is sketched in Figure 2.6. If the χ^2_{red} value exceeds a certain threshold, the algorithm stops. Alternatively, it stops, if the χ^2_{red} increases more than a predefined factor. The last point in the fit range up to which the χ^2_{red} is considered as good is declared as the last linear point. The point for which the χ^2_{red} worsens either relatively or absolutely is defined as the first non-linear point.

The algorithm characterises the TT accordingly to Subsection 2.1.2. If the first non-

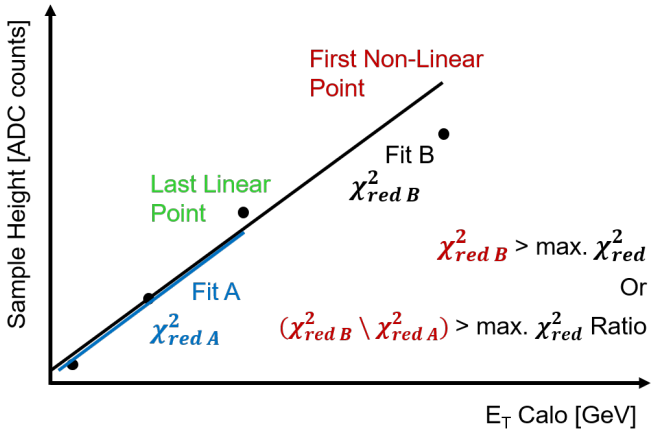

Figure 2.6.: Sketch of the χ^2_{red} threshold algorithm.

linear point sample height $\overline{\text{Point}}$ is equal to or greater than 1020 ADC counts, the TT is classified as *linear until saturation*. If the last linear fit includes the last data point, the TT is characterised as *linear and not saturated*. Else, the TT is defined as *not linear*.

2.4. Threshold Determination

This section describes the threshold determination for the residual threshold algorithm and the χ^2_{red} threshold algorithm. Both algorithms are calibrated for the pulser runs for the Run 2 system with a 40 MHz digitisation frequency for the time slices n and n-1. The χ^2_{red} method uses the residual algorithm performance criteria to obtain an equal linearity sensitivity and to provide a cross check for the residual based linearity characterisation.

2.4.1. Residual Threshold Determination

Choosing the maximal allowed residual deviation for the first point not included in the fit range must take the uncertainty in the sample height and $E_{\mathrm{T}}^{\mathrm{Calo}}$ into account. A cut on a residual of 20 ADC counts is chosen and validated in this subsection. An example for a first non-linear point deviating approximately with 20 ADC count for time slice n-1 is given in Figure 2.7.

Figure 2.8 shows the residual distribution for the first non-linear point excluding saturated TT sfor the chosen threshold of 20 ADC counts and for a lower threshold of 10 ADC counts. For both cuts, the residual distributions are approximately Gaussian distributed around 0 ADC counts. The width for the 10 ADC count cut can be estimated to approximate 20 ADC counts in Figure 2.8a. Figure 2.8b depicts the chosen residual cut with the Gaussian distribution cut out.. The definition of the residual is chosen as such, that a point deviates with a positive residual, if the points lies underneath the fit or the extrapolation. It is expected that for a saturating TT the pulser run data points will

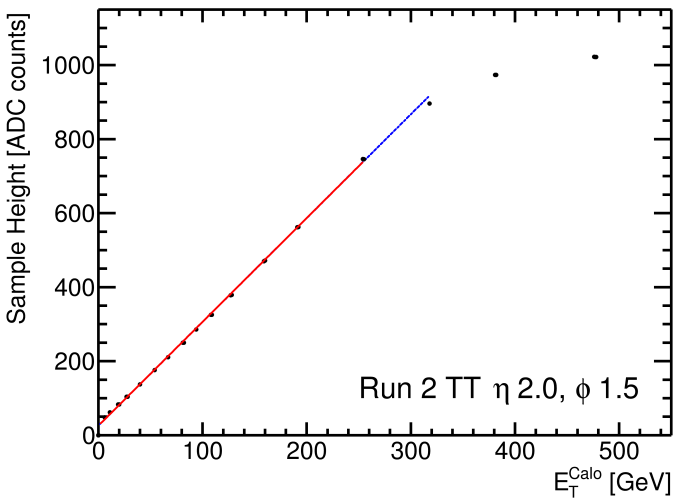

Figure 2.7.: Residual threshold 20 ADC counts, Run 2 system, time slice n-1. The fit is shown in red, the extrapolation for the first point not included in the fit range in blue. The residual for the first point not included in the fit range is ≈ 20.9 ADC counts.

deviate underneath the so far fitted points. The residual distribution for the chosen cut of 20 ADC counts shows more positive than negative entries. This indicates the correct determination of the first non-linear point with the threshold of 20 ADC counts. The threshold choice of 20 ADC counts is further checked for time slice n-1 in Figure A.1. The residual distribution show similar behaviour as for time slice n.

Furthermore, the residual and the $E_{\mathrm{T}}^{\mathrm{Calo}}$ deviation for the last linear point are analysed for the chosen threshold of 20 ADC counts. Figure 2.9 shows the distributions for the residual and the $E_{\mathrm{T}}^{\mathrm{Calo}}$ deviation for the last linear point for time slice n. Figure 2.9a depicts that the most last linear points have a residual within $\pm$ 8 ADC counts. The approximately Gaussian distributed residuals have a peak at 1 ADC count. This demonstrates, that the with a cut on 20 ADC counts for the first non-linear point the last linear point lie close to the fit. The trend to positive residual and $E_{\mathrm{T}}^{\mathrm{Calo}}$ deviation values is seen for the last linear point, too. In addition, it can be seen, that one ADC counts corresponds to an $E_{\mathrm{T}}^{\mathrm{Calo}}$ of approximately 0.25 GeV as expected. Figure A.2 maps the deviations for the TTs in the EM calorimeter. The larger deviations are obtained for TTs in the FCal.

The residual and the $E_{\mathrm{T}}^{\mathrm{Calo}}$ deviation for the last linear points for time slice n-1 are given in Figure A.3. For the EMB and EMEC outer wheel, the TTs show a similar behaviour to time slice n. The FCal and EMEC inner wheel show negative residuals close to the threshold for the last linear point.

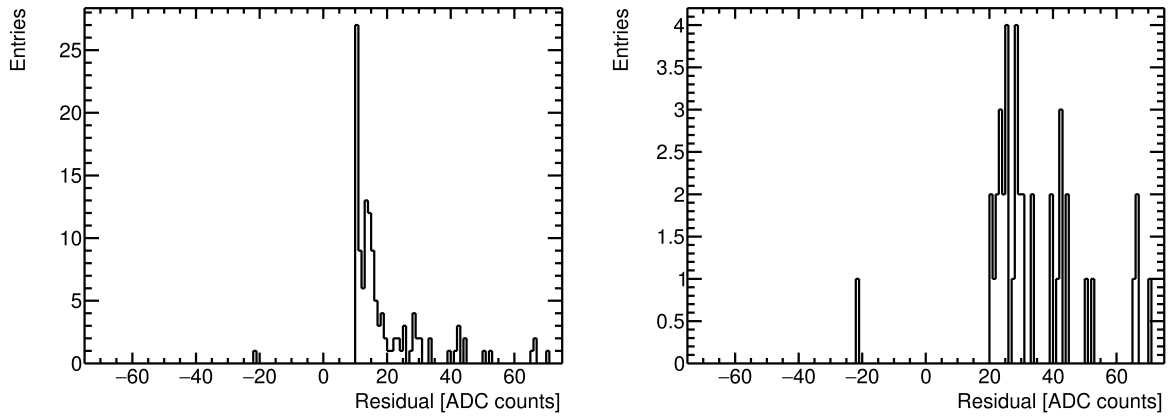

(a) Residual threshold 10 ADC counts.

(b) Residual threshold 20 ADC counts.

Figure 2.8.: Residual distribution for the NLP excluding all saturated TTs for the residual method with thresholds 10 and 20 ADC counts, Run 2 system, time slice n.

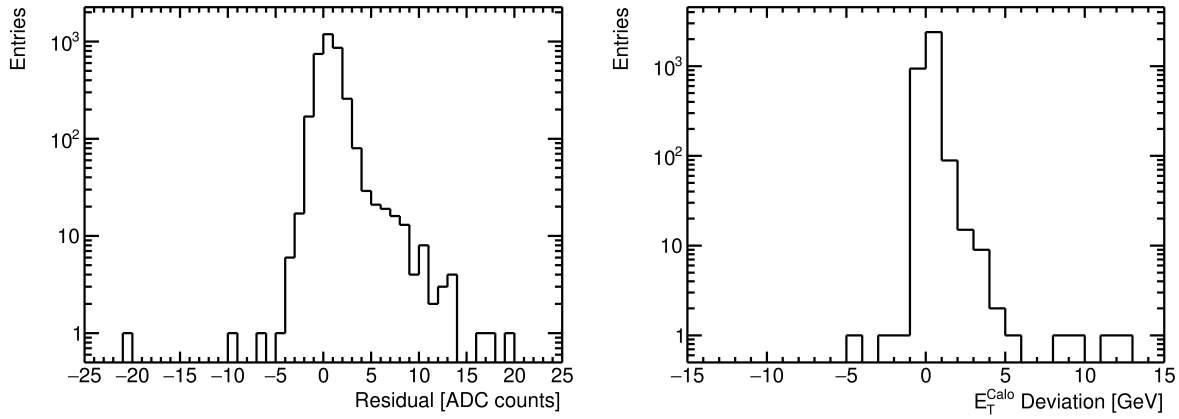

(a) Residual deviation LLP.

(b) $E_{\mathrm{T}}^{\mathrm{Calo}}$ deviation LLP.

Figure 2.9.: Residual and $E_{\mathrm{T}}^{\mathrm{Calo}}$ deviation for LLP for the residual method with a threshold of 20 ADC counts, Run 2 system, time slice n.

2.4.2. Chi Squared Reduced Threshold Determination

The χ^2_{red} threshold algorithm is used to cross check the residual based algorithm performance. The χ^2_{red} threshold determination is oriented at the χ^2_{red} distributions for the residual threshold algorithm with a cut on 20 ADC counts.

The methods defines a non-linear fit, if the χ^2_{red} is greater than 20 or the χ^2_{red} worsens more than by the factor of 10 for to consecutive fit ranges. For the non-liner fit, a minimal χ^2_{red} of 2 is enforced to avoid the false characterisation of non-linearities which are found by the impair factor. The χ^2_{red} thresholds are validated for the Run 2 system, time slices n and n-1.

In Figure 2.10 the χ^2_{red} distributions for the last linear fit obtained by the residual method are given for time slices n and n-1. Figure 2.10a shows the distribution for time slice n. The distribution is peaked at a χ^2_{red} of 0.5. The tail ends at a χ^2_{red} of 12. For time slice n-1, Figure 2.10b, the χ^2_{red} distribution peaks at 3, the tail reaches a χ^2_{red} of 25.

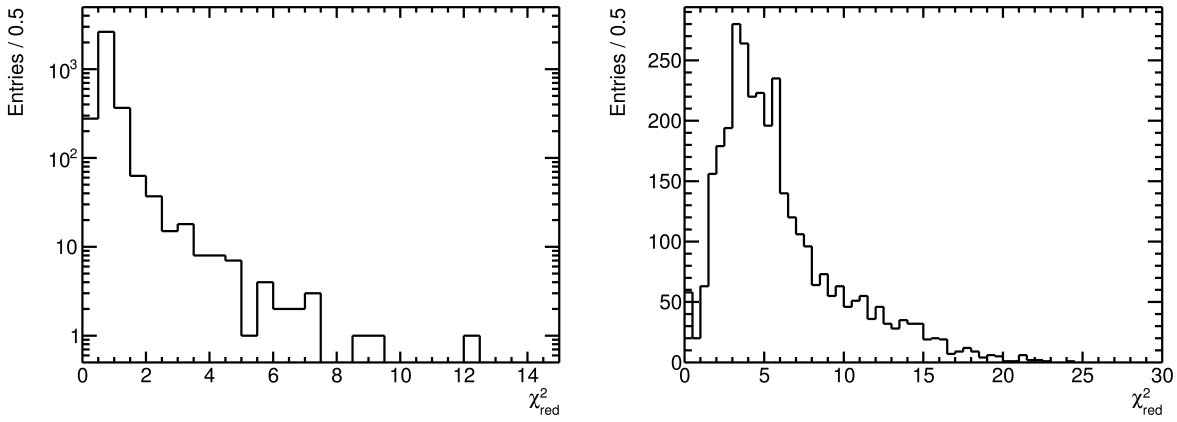

(a) Time slice n.

(b) Time slice n-1.

Figure 2.10.: χ^2_{red} distributions for the last linear fit for the residual method with a threshold of 20 ADC counts, Run 2 system, time slices n and n-1.

Figure 2.11 shows the χ^2_{red} distributions for the first non-linear fit obtained with the residual method for the chosen cuts for time slices n and n-1. All entries below a χ^2_{red} of 20 result from the cut on the consecutive χ^2_{red} comparison. The relative χ^2_{red} cut identifies more non-linearities for time slice n than for slice n-1. For time slice n-1, the absolute cut on a χ^2_{red} of 40 can be seen clearly. The χ^2_{red} distributions for the last linear fit are given in Figure A.4. They resemble the χ^2_{red} distributions for the residual threshold algorithm.

A further check for the χ^2_{red} threshold determination is given by the residual and $E_{\mathrm{T}}^{\mathrm{Calo}}$ deviation for the last linear point and the first non-linear point. They are shown for both methods for the time slices n and n-1 in Figures A.5 and A.6. The residual and the

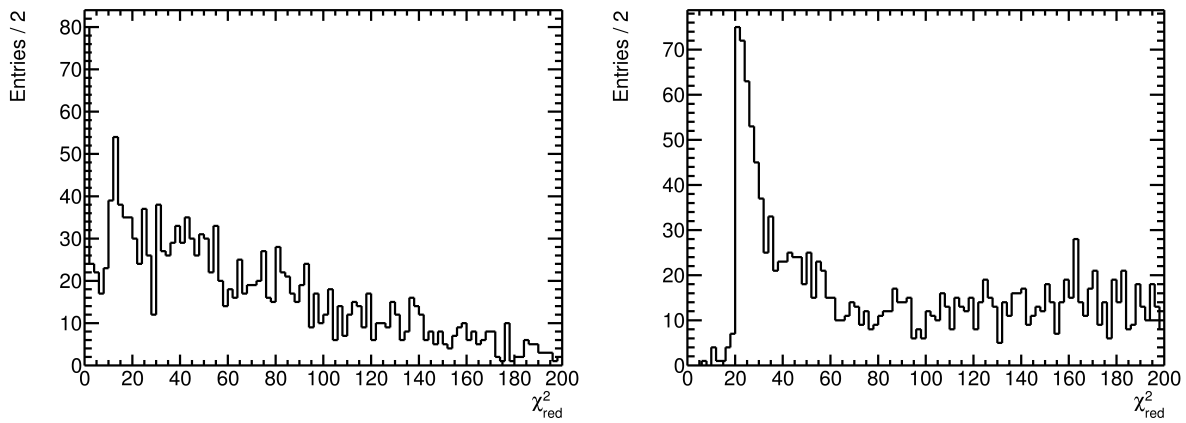

(a) Time slice n. (b) Time slice n-1.

Figure 2.11.: χ^2_{red} distributions for the first non-linear fit obtained by the χ^2_{red} method with a maximal absolute χ^2_{red} of 40 and a maximal worsening by the factor of 10, Run 2 system, time slices n and n-1.

$E_{\mathrm{T}}^{\mathrm{Calo}}$ deviation show similar behaviour as for time slice n for the last linear and the first non-linear point. For the χ^2_{red} threshold algorithm, the absence of a cut on the residual is seen for the residual and because of the correlation also no cut for the $E_{\mathrm{T}}^{\mathrm{Calo}}$ deviation.

The residual threshold and the χ^2_{red} threshold algorithms are approximate equally sensitive regarding non-linearities. The χ^2_{red} method will be used as a restricted check since the cuts on the χ^2_{red} are tuned with the residual threshold algorithms performance.

3. Results

This chapter summarizes the results of the Level-1 Calorimeter Trigger saturation studies. The trigger tower (TT) linearity characterisation is performed for the Run 2 system and the one upgraded LTDB corresponding to 16 TTs at ($1.6 \leq \eta \leq 2.5$), ($\frac{3\pi}{8} \leq \phi \leq \frac{4}{8}$) during the Phase-I Upgrade. The residual method applies a cut on the residual at 20 ADC counts. The χ^2_{red} method identifies a non-linearity for a χ^2_{red} greater than or equal to 20 or for a relative worsening of the χ^2_{red} for two consecutive fit ranges by a factor greater than or equal to 10.

For the Run 2 system the linearity characterisation is compared for the residual threshold algorithm and the χ^2_{red} threshold algorithm. The Run 2 system performs a 40 MHz digitisation frequency, therefore the three time slices n, n-1 and n-2 are analysed.

The TT linearity characterisation for the new LTDB is compared with the Run 2 system for the residual threshold algorithm for time slices n, n-1 and n-2. The the Run 2 linearity definition with a maximal residual deviation of 20 ADC counts is applied. The new system uses a 80 MHz digitisation frequency. Lacking an equivalent in the Run 2 system, the TT linearity characterisation for the intermediate time slices n-0.5 and n-1.5 are attached in Figure B.10.

The new analog signal path modified by the new Layer Sum Boards influences the signal latency in total by circa 6-10 ns. The signals from the calorimeter layer 0 and layer 3 have the same latency as the Run 2 system. Layers 1 and 2 signals are delayed by several nanoseconds. Figure 3.1a demonstrates that the delayed signal is digitised 6 to 10 ns earlier than it was in Run 2. For the same signal height, lower sample heights are measured. The sample heights before and after the upgrade are shown for one TT in Figure 3.1b. In addition to the absolute value change, the latency changes the proportionality for $E_{\mathrm{T}}^{\mathrm{Calo}}$ and sample height, too. Therefore, the sample heights and $E_{\mathrm{T}}^{\mathrm{Calo}}$ and thus the residual and $E_{\mathrm{T}}^{\mathrm{Calo}}$ deviations for the new LTDB are not directly comparable to the Run 2 system.

The overlap region $\eta \pm 1.6$ is excluded and therefore appears blank in all Figures. The pulser runs for the TTs at $-0.8 \leq \eta \leq -0.4$, $\phi = 3$ malfunctioned due to broken electronics and are therefore not linear.

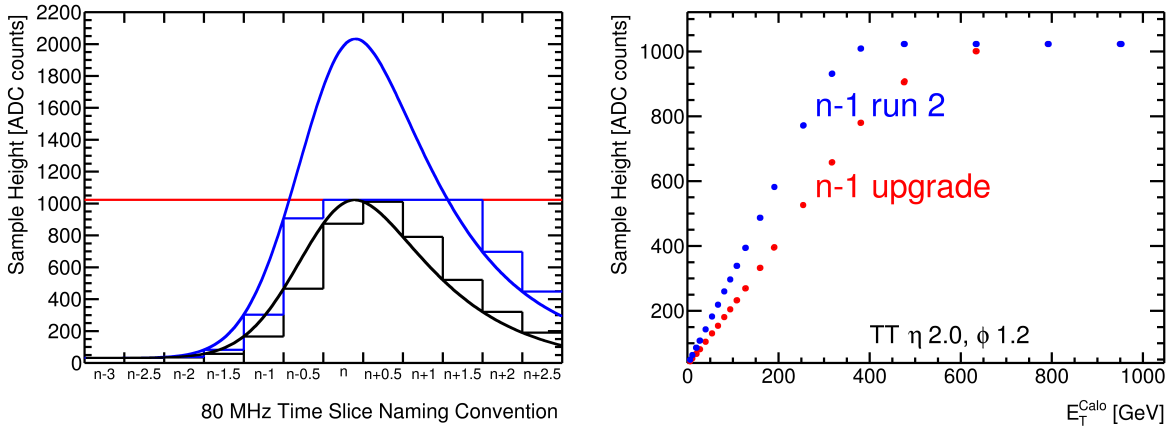

(a) 80 MHz digitisation for the 10 ns delayed signal with half-integer time slice naming convention, in black for a low charge signal, in blue for a high charge signal exceeding the maximal digital sample height of 1023 ADC counts, drawn in red.

(b) Pulser run for trigger tower at $\eta = 2.0$, $\phi = 1.2$, Run 2 system in blue and in red after the Phase-I Upgrade.

Figure 3.1.: Phase-I Upgrade delayed signal digitisation and influence on the pulser run.

3.1. Time Slice n

Run 2 System Linearity Characterisation

Figure 3.2 presents the TT linearity classification for Run 2 for time slice n. Figure 3.2a shows the findings obtained by the residual threshold algorithm, the characterisation based on the χ^2_{red} thresholds is depicted in Figure 3.2b.

The residual method characterises the majority of TTs in the EMB and EMEC outer wheel to be linear until saturation, coloured in green. This classification is given by time slice n containing the signal peak. Therefore, for $E_{\mathrm{T}}^{\mathrm{Calo}} \gtrsim 250\,\mathrm{GeV}$ the maximal analog-to-digital converter sample height of 1023 ADC counts cuts is exceeded by the signal.

The EMEC inner wheel TTs are characterised linear but not saturated, shown in blue. A TT in the EMEC region contains fewer calorimeter cells than in the central or outer region. Hence, the Trigger Tower Builder Board sums up fewer cells and the TT signal does not saturate by the injected pulses. The outermost TTs of the FCal at $\eta \pm 4.9$ are characterised linear but not saturated, too. Given the large η, the charge injections do not convert into high enough $E_{\mathrm{T}}^{\mathrm{Calo}}$ to saturate.

Not linear characterised TTs are coloured in orange and red, allowing a sub-characterisation in slightly and highly not linear TTs. Orange means an absolute residual deviation smaller or equal to 30 ADC counts (and greater or equal to 20 ADC counts). TTs with absolute residual deviation greater than 30 ADC counts are depicted in red.

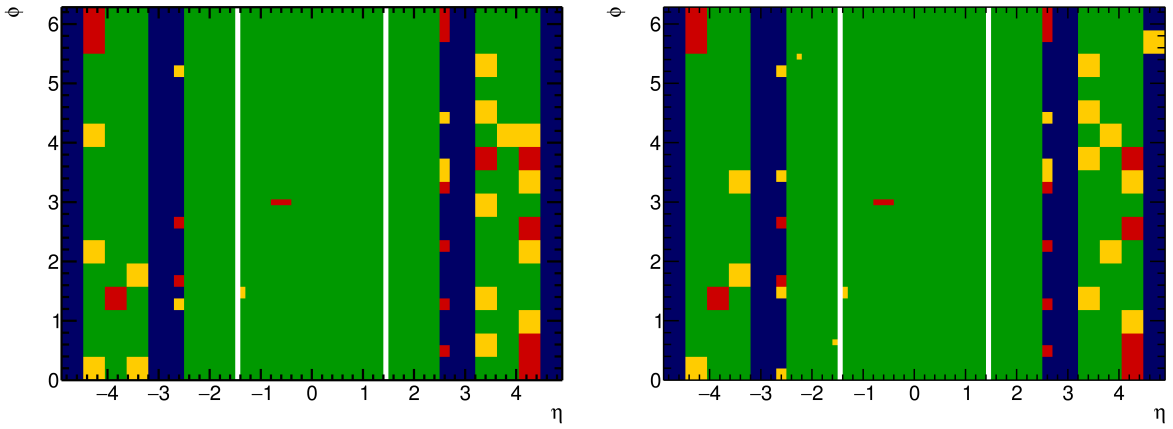

(a) Residual threshold algorithm.

(b) χ^2_{red} threshold algorithm.

Figure 3.2.: TT linearity characterisation with both methods, Run 2 system, time slice n.
TT linearity categories: linear until saturation – green, linear and not saturated – blue, not linear with $20 \leq |\text{residual}| \leq 30$ – orange, not linear with $|\text{residual}| > 30$ – red. All values in ADC counts.

For the EMEC inner wheel at $\eta \pm 2.5$ and in the outer region the residual method identifies several slightly not linear TTs and few highly not linear TTs.

The χ^2_{red} method confirms the TT linearity characterisation obtained by the residual method, see Figure 3.2b. The EMB and EMEC outer wheel are found to be in general linear until saturation. The EMEC inner wheel and the outermost FCal TTs at η slices are mostly characterised as linear but not saturated. Two TTs in the EMEC inner wheel are found not linear. In the FCal, the χ^2_{red} finds less not linear TT in the FCal except for the outermost FCal η slice. There, the χ^2_{red} method finds two not linear TTs.
The residual method is more stable than the χ^2_{red} algorithm because the χ^2_{red} does not detect not all non linearities which are found with residual deviations greater than 20 ADC counts by the residual cut. In addition, the χ^2_{red} cuts are optimized with regard to the residual algorithm. Given the lower sensitivity and the threshold choice, the χ^2_{red} method is used a cross check.

Figure 3.3a maps the residual deviation for the first non-linear point for all not linear characterised TTs by the residual method. The most TTs deviate less than 30 ADC counts at the first non-linear point and are therefore characterised as slightly not linear. Given the residual definition, Equation (2.2), points with positive residual deviations lie underneath the fit projection. To check whether this is because of digitisation saturation effects, the sample height for the first non-linear point is given in Figure 3.3b. It can be seen that the first non-linear point sample heights for most not linear TTs are close to 1020 ADC counts. Hence, the non linearities could result from the maximal digital sample height. Three not linear TTs at $(\eta, \phi) = (3.4, 5.3)$, $(3.4, 4.5)$ and $(3.8, 4.1)$ have

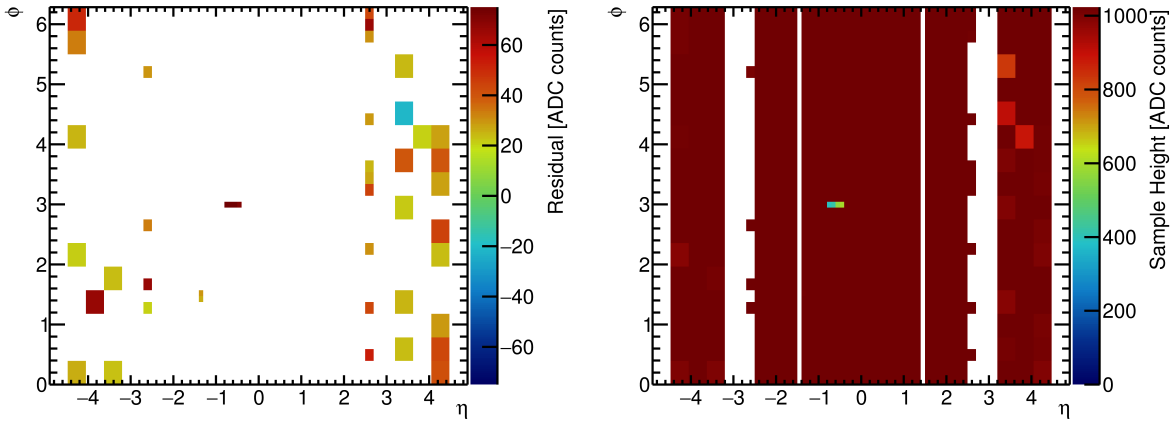

(a) Residual deviation NLP not linear TTs.

(b) Sample height NLP.

Figure 3.3.: Residual deviation for not linear TTs and sample height for the NLP for the residual method, Run 2 system, time slice n.

sample heights for the first non-linear point lower than 900 ADC counts. Therefore, these non-linearities do probably not result from digital saturation effects.

Some TTs are characterised not linear with negative residuals for the first non-linear point, because the measured sample heights lie above the linear extrapolation. Thus, the non linearity is not caused by digital saturation effects.

The residual deviation for the last linear point for all not linear TTs is given in Figure 3.4a. For most TTs, the deviation is within ±5 ADC counts, which underlines the definition as a *linear* point. Comparing the residuals for the last linear and the first non linear point for all not linear TTs demonstrates that the residual for the first non-linear point is always greater than for the last linear point.

An additional cut on the sample height would require thorough care for the η dependency of the sample height. The sample height for the last linear and the first non-linear point are shown in Figure 3.4b and Figure 3.3b. Pulser runs for TTs characterised as linear but not saturated do not contain a first non-linear point. Therefore they appear blank in Figure 3.3b.

The $E_{\mathrm{T}}^{\mathrm{Calo}}$ values for the first non-linear and the last linear point for time slice n obtained by the residual method are attached in Figure B.1. The $E_{\mathrm{T}}^{\mathrm{Calo}}$ deviations for the first non linear and the last linear point for all not linear TTs are given in Figure B.2. The correlation of sample height and $E_{\mathrm{T}}^{\mathrm{Calo}}$ with approximately 1 ADC count for 0.25 GeV can be seen. Therefore, the findings discussed for the sample height and the residual are applicable equivalently for $E_{\mathrm{T}}^{\mathrm{Calo}}$ values and the $E_{\mathrm{T}}^{\mathrm{Calo}}$ deviation. For the first non-linear points, a residual of approximately 20 ADC counts is equivalent to a $E_{\mathrm{T}}^{\mathrm{Calo}}$ deviation of circa 5 GeV. Positive/ negative residuals translate into positive/ negative $E_{\mathrm{T}}^{\mathrm{Calo}}$ deviations.

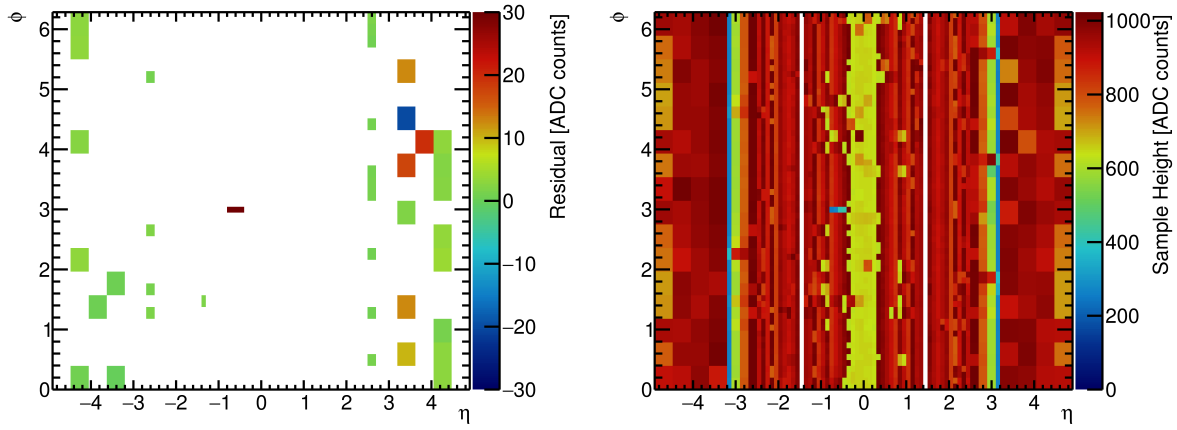

(a) Residual deviation LLP not linear TTs.

(b) Sample Height LLP.

Figure 3.4.: Residual deviation for not linear TTs and sample height for the LLP for the residual method, Run 2 system, time slice n.

Phase-I Upgrade Linearity Characterisation

Figure 3.5 shows the TT linearity classification, for the new LTDB without latency correction in Figure 3.5a and for Run 2 in Figure 3.5b. Regarding the TT linearity classification no change is seen for the upgraded system. All 16 upgraded TTs are classified linear until saturation as they are for the Run 2 system.

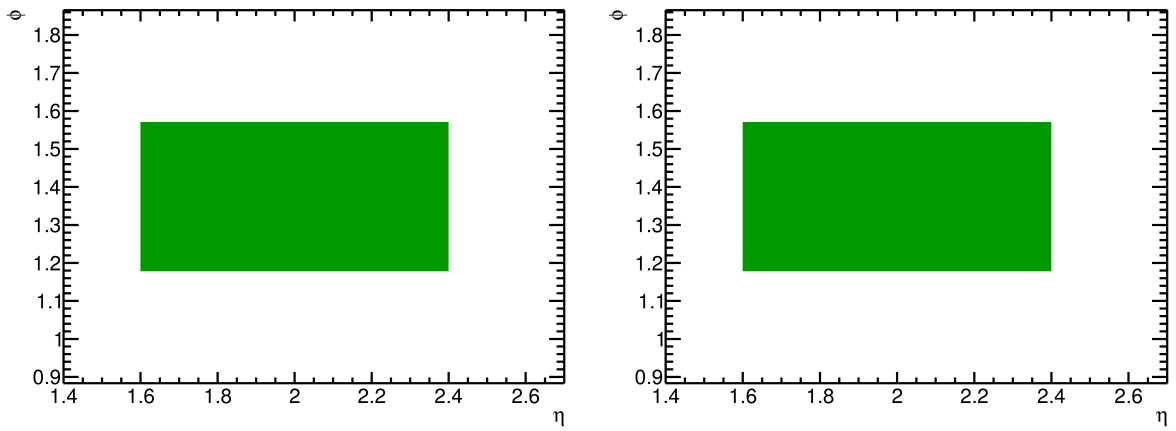

(a) Phase-I Upgrade.

(b) Run 2.

Figure 3.5.: TT linearity characterisation for the new LTDB and the Run 2 system for the residual method , time slice n. The Phase-I Upgrade signal latency is not corrected. All TTs are classified as linear until saturation.

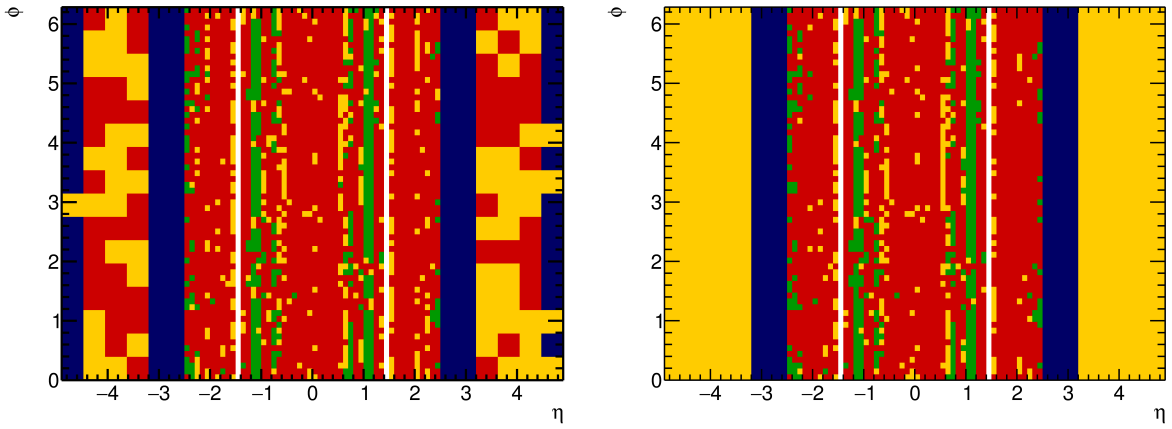

(a) Residual threshold algorithm.

(b) χ^2_{red} threshold algorithm.

Figure 3.6.: TT linearity characterisation with both methods, Run 2 system, time slice n-1.
TT linearity categories: linear until saturation – green, linear and not saturated – blue, not linear with $20 \leq |\text{residual}| \leq 30$ – orange, not linear with $|\text{residual}| > 30$ – red. All values in ADC counts.

3.2. Time Slice n-1

Run 2 System Linearity Characterisation

For the Run 2 system, time slice n-1, the TT linearity classification is given in Figure 3.6 for both methods. Figure 3.6a depicts the findings obtained with the residual threshold algorithm, Figure 3.6b shows the characterisation by the χ^2_{red} routine. For time slice n-1, most TTs in the EMB and EMEC outer wheel are characterised as not linear by both methods. For $(0.7 < |\eta| < 1.3)$ and $(2.2 < |\eta| < 2.6)$ several TTs are characterised as linear until saturation. At $|\eta| = 1.2$ the TTs are linear until saturation for almost the full ϕ coverage. All TTs in the EMEC inner wheel are linear but not saturated. Most of the outermost FCal TTs are linear but not saturated, too. Few TTs are slightly not linear.

The TT linearity characterisation obtained by the χ^2_{red} method deviates in the FCal from the residual based characterisation. The χ^2_{red} method finds non-linearities in the FCal for low sample heights because the points fluctuate for low injected charges. The sample height and the residual deviations are given in Figure B.4. Figure B.4b demonstrates that the χ^2_{red} method shows very small residual deviations for the first non-linear point. In comparison with Figure 3.7b, Figure B.4a shows the χ^2_{red} method stops at too low sample heights. This behaviour supports the usage of the χ^2_{red} method restricted to a cross check but not as an independent method.

In Figure 3.7a, the residual deviation for the first not linear point for all not linear TTs obtained with the residual method is given. The not linear characterised TTs in

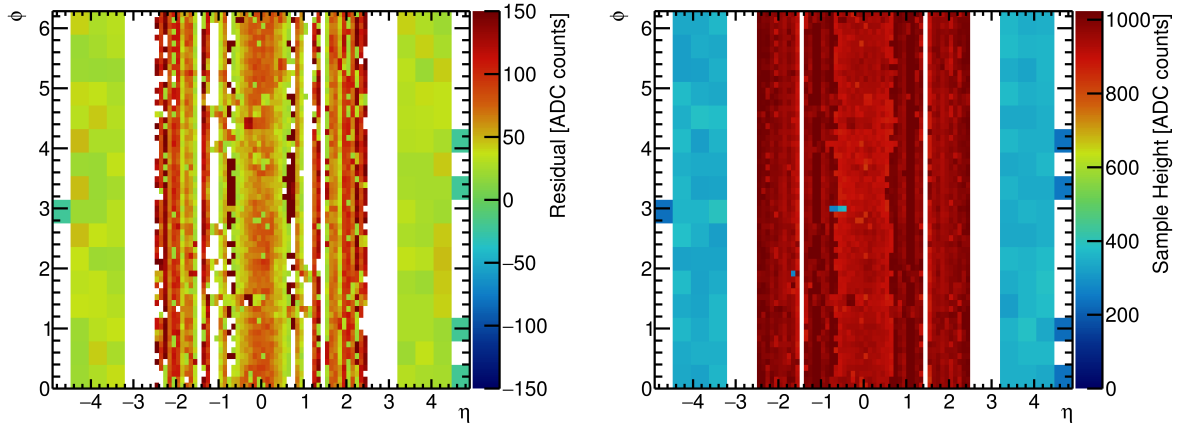

(a) Residual deviation NLP not linear TTs.

(b) Sample height NLP.

Figure 3.7.: Residual deviation for not linear TTs and sample height for the NLP, for the residual method, Run 2 system, time slice n-1.

the EMB and EMEC outer wheel have large residual deviations for the first non-linear point. Most TTs deviate more than 50 ADC counts.

In the EMEC inner wheel and FCal, the TTs deviate less than 40 ADC counts, only few deviate less than 30 ADC counts. For time slice n-1, the rising edge is digitised. Therefore, the pulse must be much larger to get a a sample height of greater than 1020 ADC counts. Thus, more saturation effects are seen for time slice n-1 because they appear for lower sample heights than for time slice n.

The small residual deviations for the last linear point for all not linear TTs is given in Figure B.3a. The deviations are smaller in the EMB and EMEC outer wheel. The TTs in the FCal and EMEC inner wheel become non linear more rapidly compared to the EMB and EMEC outer wheel. There, some last linear points deviate from the fit up to 15 ADC counts and for the first non-linear point by up to 50 ADC counts.

Similar to time slice n, some TTs characterised as non linear have negative residuals for the first non linear and last linear point. These non linearities are not caused by the studied saturation effects because the points lie above the extrapolation.

Figure 3.7b maps the sample height for the first non-linear point. In the EMB and EMEC outer wheel, the TTs become non linear close to the maximal sample height, whereas in the EMEC inner wheel and FCal they become non linear for significant lower sample heights but larger $E_{\mathrm{T}}^{\mathrm{Calo}}$ values at circa 350 GeV. The $E_{\mathrm{T}}^{\mathrm{Calo}}$ for the first non-linear and the last linear point are attached in Figure B.5.

The $E_{\mathrm{T}}^{\mathrm{Calo}}$ and $E_{\mathrm{T}}^{\mathrm{Calo}}$ deviations for the first non-linear and the last linear point for time slice n obtained by the residual method are attached in Figures B.5 and B.6.

Phase-I Upgrade Linearity Characterisation

The TT linearity classification for the Phase-I Upgrade without latency correction is given in Figure 3.8a. The corresponding findings for Run 2 are seen in Figure 3.8b.

All Phase-I upgraded TTs are characterised not linear similar to Run 2. The sub-characterisation in highly and slightly not linear TTs can only be partially compared given the not corrected signal latency, which influences the measured sample heights.

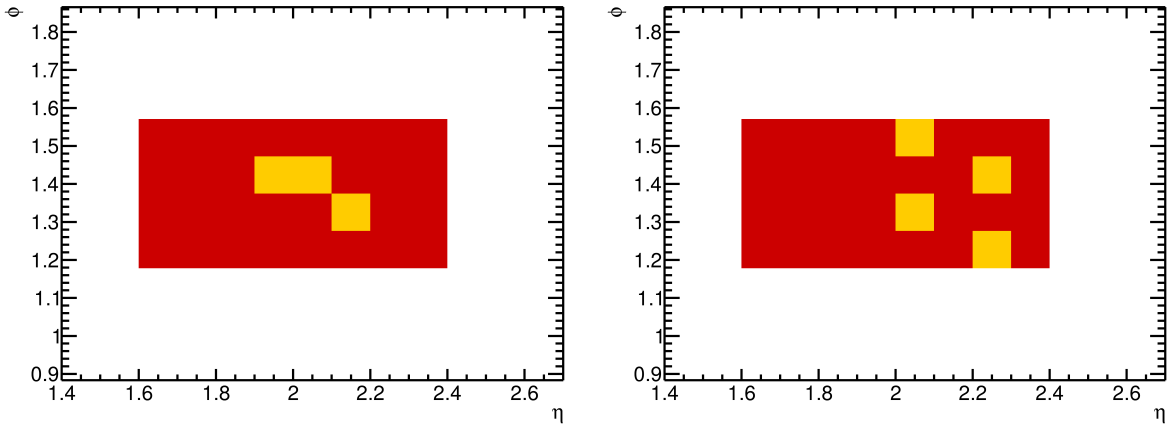

(a) Phase-I upgraded TTs.

(b) Corresponding Run 2 TTs.

Figure 3.8.: TT linearity characterisation for the new LTDB and the Run 2 system for TTs installed at the time of this thesis for the residual method with residual threshold 20 ADC counts, time slice n-1. The Phase-I Upgrade signal latency is not corrected.
TT characterisation: not linear with $20 \leq |\text{residual}| \leq 30$ – orange, not linear with $|\text{residual}| > 30$ – red. All TTs are classified not linear.

3.3. Time Slice n-2

Run 2 System Linearity Characterisation

Figure 3.9 presents the TT linearity characterisations for time slice n-2. Figure 3.9a shows the characterisation based on the residual threshold. The χ^2_{red} method findings are given in Figure 3.9b.

For time slice n-2, the EMB and EMEC outer wheel region are characterised mostly not linear. There, some TTs are characterised linear but not saturated. The EMEC inner wheel and the FCAL is mainly linear but not saturated. The residual method characterises most TTs at $(1.0 < |\eta|1.4)$ and $|\eta| = 2.4$ highly not linear. The χ^2_{red} method confirms the highly not linear TT in the EMEC inner wheel and the FCAL region. In the EMB and EMEC outer wheel, the TTs are characterised not linear because the χ^2_{red}

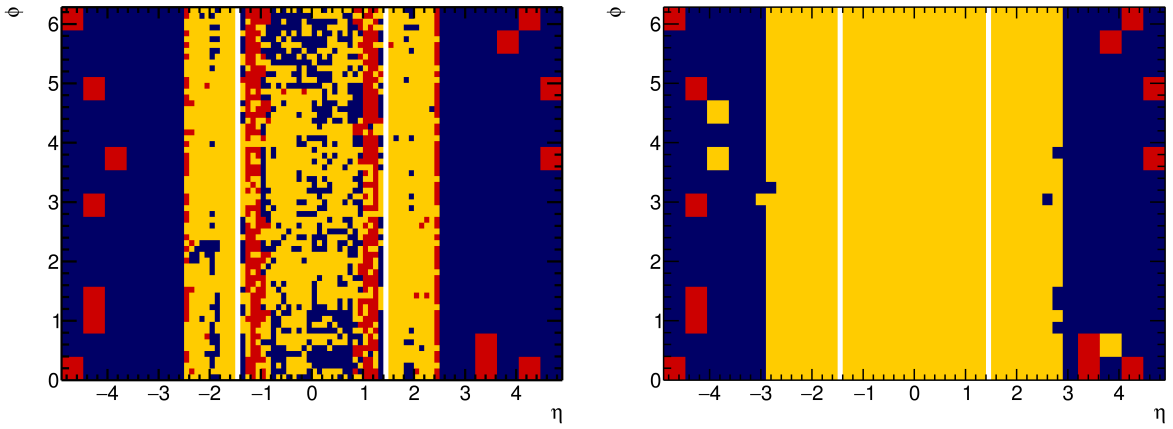

(a) Residual threshold algorithm.

(b) χ^2_{red} threshold algorithm.

Figure 3.9.: TT linearity characterisation with both methods, Run 2 system, time slice n-2.
TT linearity categories: linear until saturation – green, linear and not saturated – blue, not linear with $20 \leq |\text{residual}| \leq 30$ – orange, not linear with $|\text{residual}| > 30$ – red.

worsening factor is exceeded for the initial variations and overlapping data points.

Figure 3.10a shows the mostly negative residual deviations for all not linear TTs for the first non-linear point. In combination with the sample heights, Figure 3.10b, it is seen, that the most TTs in the EMB and EMEC outer wheel are far from saturation. For $(1.0 < \eta < 1.4)$ and $|\eta| = 2.4$, the pulser runs have sample heights of 800 ADC counts for the first non-linear point and deviate more than 30 ADC counts.

Figure B.7a shows the small residual deviations for the last linear point for all not linear TTs. Except for few TTs in the outer region, the last linear points deviate less than 10 ADC counts from the fit.

The $E_{\mathrm{T}}^{\mathrm{Calo}}$ and $E_{\mathrm{T}}^{\mathrm{Calo}}$ deviations for the first non-linear and the last linear point for time slice n obtained by the residual method are attached in Figure B.8 and B.9. Sample height and $E_{\mathrm{T}}^{\mathrm{Calo}}$ are correlated, thus the findings translate from the sample height and residual to the $E_{\mathrm{T}}^{\mathrm{Calo}}$ and $E_{\mathrm{T}}^{\mathrm{Calo}}$ deviations.

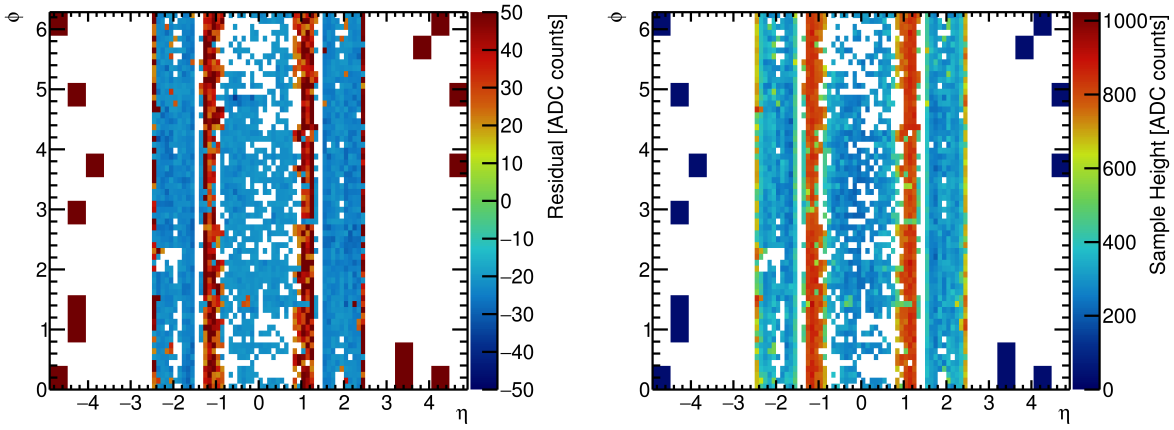

(a) Residual deviation NLP not linear TTs.

(b) Sample height NLP.

Figure 3.10.: Residual deviation for not linear TTs and sample height for the NLP, for the residual method, Run 2 system, time slice n-2.

Phase-I Upgrade Linearity Characterisation

Figure 3.11 shows the TT linearity classification for time slice n-2. The characterisation after the Phase-I upgrade without signal latency correction is given in Figure 3.11a, for Run 2 it is seen in Figure 3.11b.

The Phase-I upgraded TTs are mostly found slightly not linear with an absolute residual in the range of 20 to 30 ADC counts. In comparison with the Run 2 characterisation this behaviour is expected. Six TTs at $\eta = 1.6$ and $\eta = 1.7$ are characterised linear until saturation. This could be an artefact of the latency which reduces the slope and therefore the proportionality between the sample height and the $E_{\mathrm{T}}^{\mathrm{Calo}}$ values. Hence, the linearity threshold of 20 ADC cuts looser for the not re-timed digitisation as the sample height is smaller for the same $E_{\mathrm{T}}^{\mathrm{Calo}}$.

The Level-1 Calorimeter Saturation Studies analyses the trigger tower linearity for the readout electronics as used in Run 2. The time slices n, n-1 and n-2 are characterised in three linearity categories: linear until saturation, linear but not saturated and not linear. Not linear TTs are further distinguished by the residual for the first non-linear point in highly and slightly not linear.

The characterisation of the TTs corresponding to newly installed LTDB has not found any significant change in the linearity of pulses which cannot be traced back to the new signal path latency. The linearity studies of the Run 2 trigger towers provide a commissioning reference once more LTDBs are installed and the analog signal paths are synchronized for the different layers by the Tower Builder Boards.

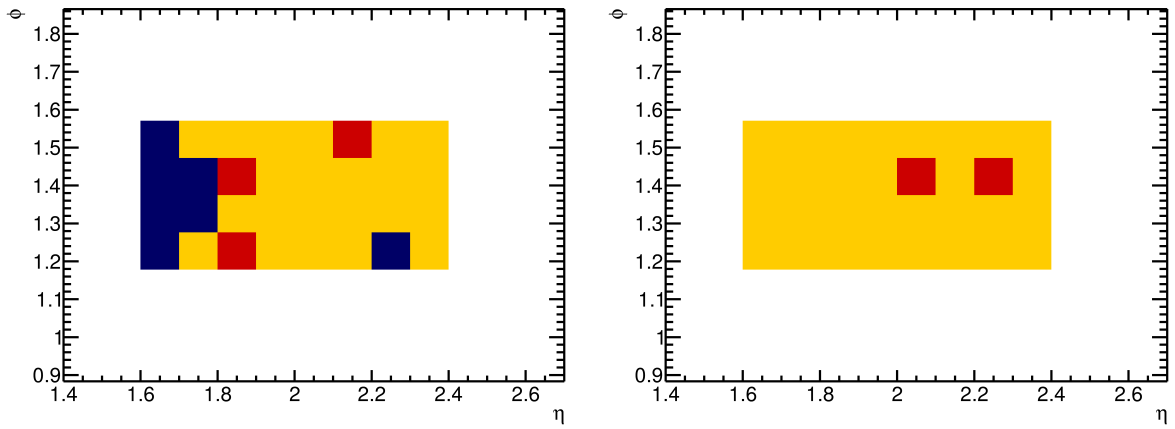

(a) Phase-I upgraded TTs.

(b) Corresponding Run 2 TTs.

Figure 3.11.: TT linearity characterisation for the new LTDB and the Run 2 system for TTs installed at the time of this thesis for the residual method with residual threshold 20 ADC counts, time slice n-2. The Phase-I Upgrade signal latency is not corrected.
TT characterisation: linear but not saturated – blue, not linear with $20 \leq |\text{residual}| \leq 30$ – orange, not linear with $|\text{residual}| > 30$ – red. All TTs are classified not linear.

4. Conclusion

The LAr calorimeter Phase-I upgrade provides an increased granularity in η, and longitudinal shower information. Therefore, the Run 2 trigger towers real time path is modified by the new Layer Sum Boards and LAr Trigger Digitizer Boards (LTDBs). The signal is transmitted via a new analog signal path to the Run 2 Tower Builder Boards (TBBs). This thesis analyses the linearity of the trigger tower (TT) signal digitisation before and after the Phase-I upgrade.

The linearity of a TT is characterised in three categories: linear until saturation, linear but not saturated, and not linear. Two linear fit algorithms have been developed and calibrated with data from the Run 2 system. In addition, the absolute values and deviations from the fit regarding the sample height and $E_{\mathrm{T}}^{\mathrm{Calo}}$ are analysed.

The algorithms extend the fit range iteratively and identify the last linear and the first non-linear point for a series of pulse injections per TT. The residual method cuts on the residual of the last point included or the next point not included in the fit range. The χ^2_{red} method compares the χ^2_{red} values for two consecutive fit ranges. The χ^2_{red} thresholds are based on the residual method's performance. Therefore, it is used as a cross check for the residual method. Due to fluctuations at low $E_{\mathrm{T}}^{\mathrm{Calo}}$ values, the χ^2_{red} method is found to be less stable.

The linearity of the $E_{\mathrm{T}}^{\mathrm{Calo}}$ and ADC sample height has been investigated and the slope of approximate 4 was found as expected. For time slice n, the EMB, EMEC outer wheel and the FCal region are characterised linear until saturation. The EMEC inner wheel and the outermost FCal TTs are characterised linear but not saturated. For time slice n-1, the EMB and EMEC outer wheel region is found slightly non linear. Only the trigger towers near $|\eta| = 1$ are characterised as linear until saturation. The EMEC inner wheel and the FCal are characterised linear but not saturated. For time slice n-2, the EMB and EMEC outer wheel are found non linear with residuals in the range of 20 to 30 ADC counts, near $|\eta| = 1$ the residuals are greater than 30 ADC counts. FCal and EMEC inner wheel are characterised linear but not saturated.

So far, one LTDB corresponding to 16 TTs has been installed during the Phase-I upgrade. The new signal path latency has not been corrected yet and the signal is digitised 6 to 10 ns earlier than in Run 2. Therefore, only a qualitative linearity characterisation is possible because the digitised sample heights are not calibrated. The linearity characterisations of the new TTs are in agreement with the corresponding Run 2 system, provided that the thresholds are approximately valid for the mistimed digitisation.

The signal latency needs to be retimed at the TTBs. Once more LTDBs are installed, calibration runs for the TTBs and LTDBs can be taken. More charge injections points close to saturation would enable a new sensitivity for the non linearity characterisation.

Appendix

A. Threshold Determination

A.1. Residual Threshold Determination

Figure A.1 shows the residual deviations for the first non-linear point excluding all saturated trigger towers for threshold of 10 and 20 ADC counts for Run 2 trigger towers, time slice n-1. Similar to time slice n, the tails of the approximate Gaussian distributed. Unlike for time slice n, very few trigger towers are saturated, therefore, both distributions show more entries. The negative residuals in Figure A.1a belong almost exclusively to FCal and EMEC inner wheel TTs. Most of the very large residuals results from TTs near to the overlap region.

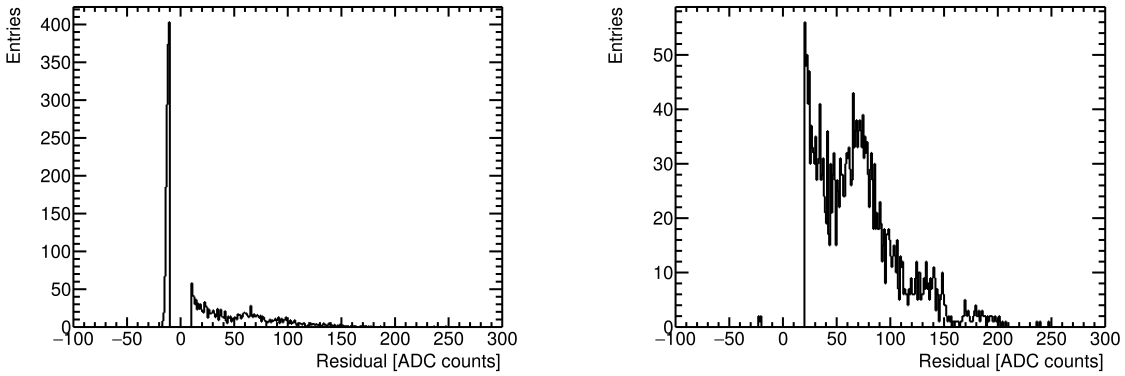

(a) Residual threshold 10 ADC counts.

(b) Residual threshold 20 ADC counts.

Figure A.1.: Residual deviations for the NLP excluding all saturated TTs for the residual method with the thresholds 10 and 20 ADC counts, Run 2 system, time slice n-1.

Figure A.3a demonstrates the cut on the residual at 20 ADC counts for the LLP. Compared to time slice n, the residual deviation is larger for time slice n-1 because the TTs are less linear. Figure A.3c depicts the large deviations in the EMEC inner wheel and FCal. Similar to slice n, the residual in the central region is close to $\pm$ 20 ADC counts.

The $E_{\mathrm{T}}^{\mathrm{Calo}}$ deviation is smaller than $\pm$ 8 GeV for most trigger towers, similar to time slice n, Figure A.3b, some FCal and EMEC inner wheel TTs deviate more than $\pm$ 10 GeV.

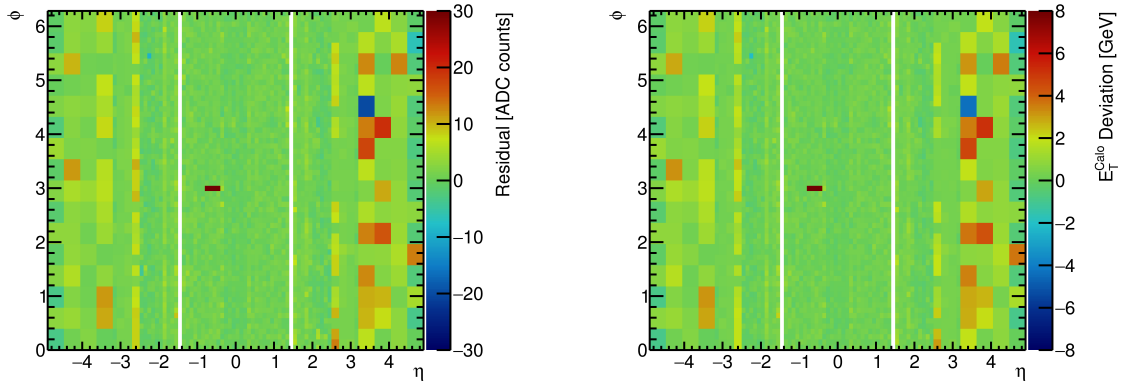

(a) Residual deviation. (b) $E_{\mathrm{T}}^{\mathrm{Calo}}$ deviation.

Figure A.2.: Residual and $E_{\mathrm{T}}^{\mathrm{Calo}}$ deviations for the LLP for the the residual method with a threshold of 20 ADC counts, Run 2 system, time slice n.

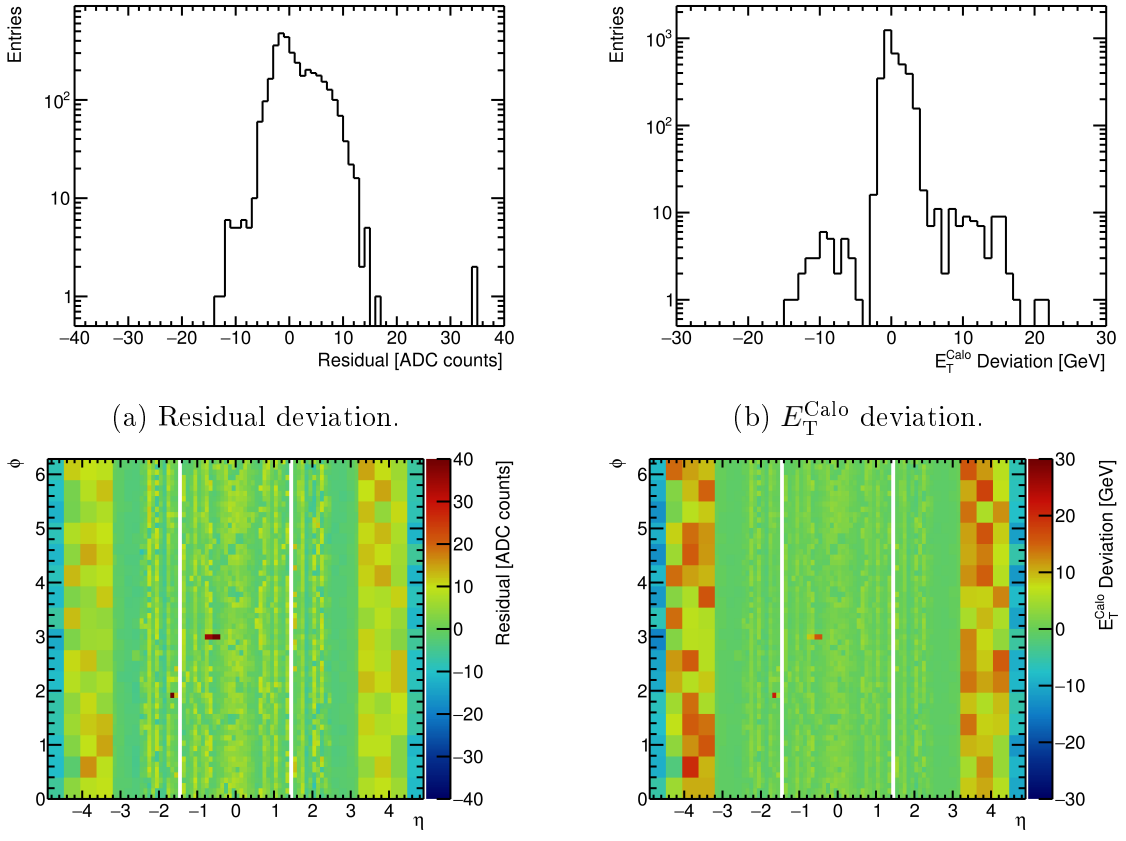

(a) Residual deviation. (b) $E_{\mathrm{T}}^{\mathrm{Calo}}$ deviation.

(c) Residual deviation. (d) $E_{\mathrm{T}}^{\mathrm{Calo}}$ deviation.

Figure A.3.: Residual and $E_{\mathrm{T}}^{\mathrm{Calo}}$ deviations for the LLP for the residual method with a threshold of 20 ADC counts, Run 2 system, time slice n-1.

A.2. Chi Squared Reduced Threshold Determination

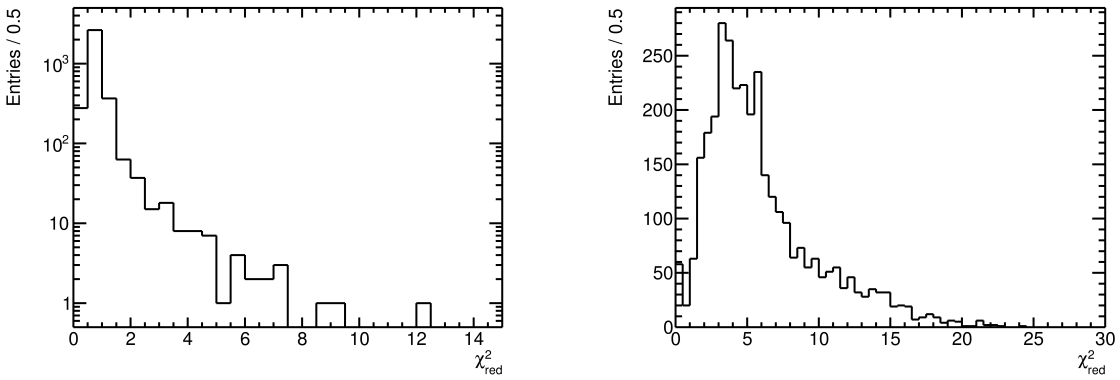

(a) Time slice n. (b) Time slice n-1.

Figure A.4.: χ^2_{red} distributions for the last linear fit obtained by the χ^2_{red} method, Run 2 system, time slices n and n-1.

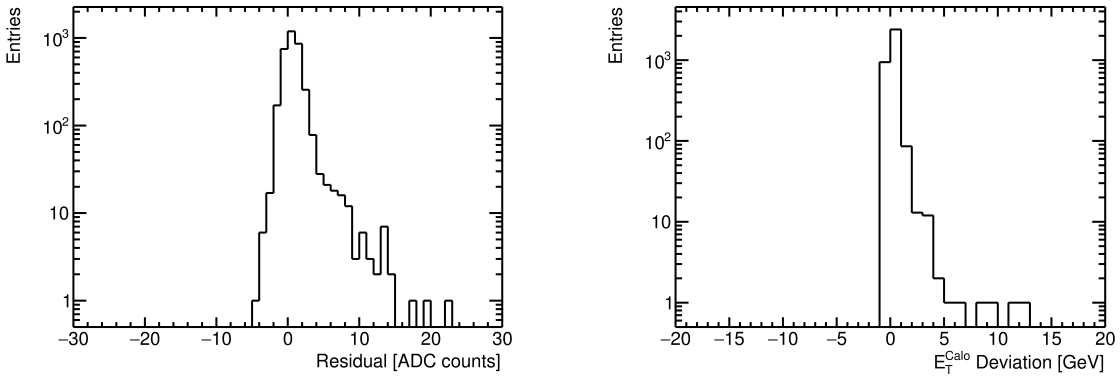

(a) Residual deviation LLP. (b) $E_{\mathrm{T}}^{\mathrm{Calo}}$ deviation LLP.

Figure A.5.: Residual and $E_{\mathrm{T}}^{\mathrm{Calo}}$ deviations for the LLP for the χ^2_{red} method with a maximal χ^2_{red} of 20 and a maximal relative worsening of 10, Run 2 system, time slice n.

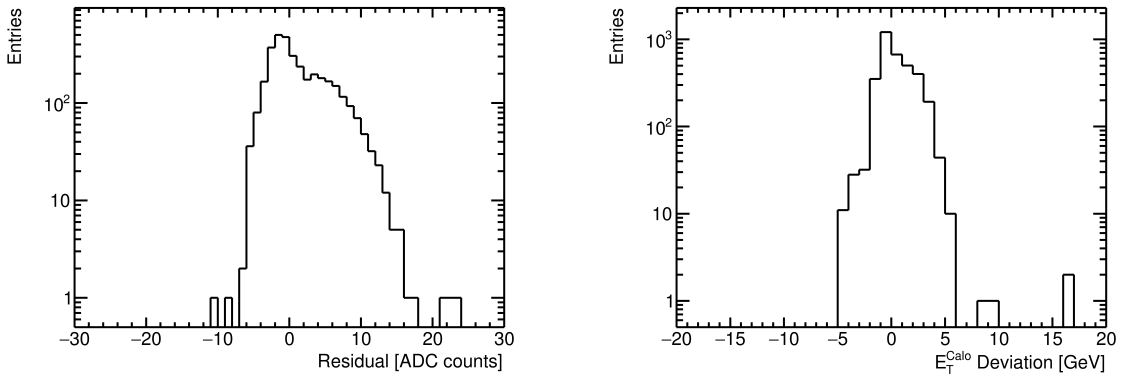

(a) Residual deviation LLP.

(b) $E_{\mathrm{T}}^{\mathrm{Calo}}$ deviation LLP.

Figure A.6.: Residual and $E_{\mathrm{T}}^{\mathrm{Calo}}$ deviations for the LLP for the χ^2_{red} method with a maximal χ^2_{red} of 20 and a maximal relative worsening of 10, Run 2 system, time slice n-1.

B. Results

B.1. Time Slice n

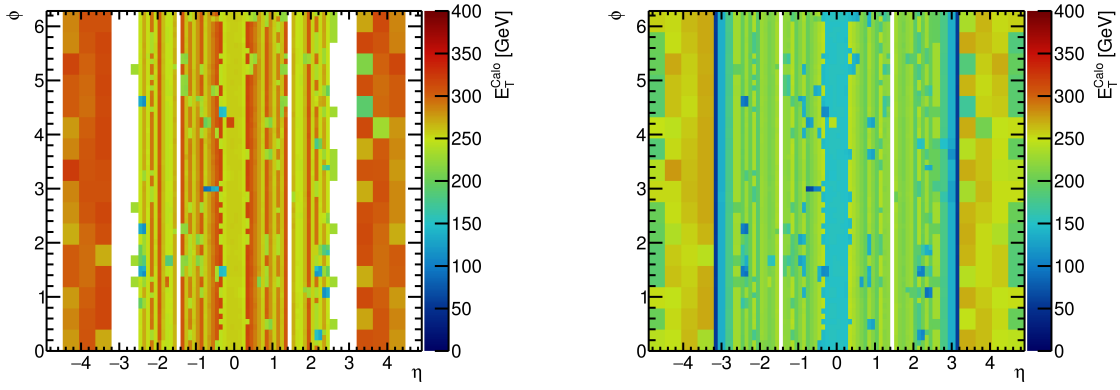

(a) $E_{\mathrm{T}}^{\mathrm{Calo}}$ NLP. (b) $E_{\mathrm{T}}^{\mathrm{Calo}}$ LLP.

Figure B.1.: $E_{\mathrm{T}}^{\mathrm{Calo}}$ values for the NLP and LLP for the residual method, Run 2 system, time slice n.

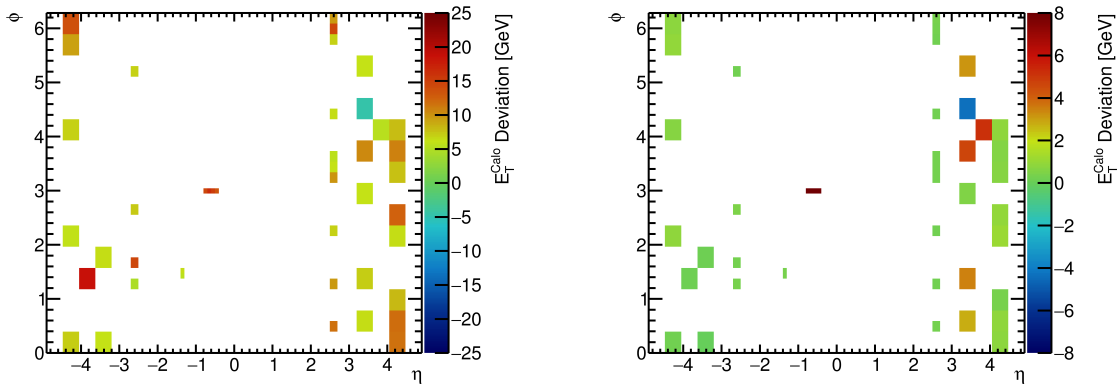

(a) $E_{\mathrm{T}}^{\mathrm{Calo}}$ deviation NLP for not linear TTs. (b) $E_{\mathrm{T}}^{\mathrm{Calo}}$ deviation LLP for not linear TTs.

Figure B.2.: $E_{\mathrm{T}}^{\mathrm{Calo}}$ deviation for the NLP and LLP for not linear TTs for the residual method, Run 2 system, time slice n.

B.2. Time Slice n-1

Figure B.3b maps the sample heights for the last linear which lie at circa 800 ADC counts. The pulser runs for the innermost η slices, $|\eta| \leq 0.2$, contain only three points with 200 events in the range of 150 GeV to 350 GeV. At time slice n, the pulser run saturates for 250 GeV, therefore, the last linear point is found at 150 GeV due to the lack of a point in between. At time slice n-1, the pulser run becomes not linear at 350 GeV, thus, the last linear point is declared at about 250 GeV.

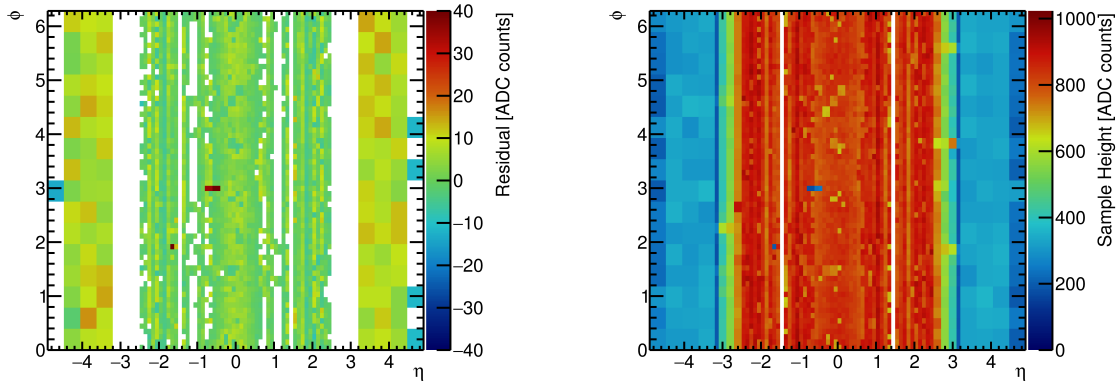

(a) Residual deviation LLP not linear TTs.

(b) Sample Height LLP.

Figure B.3.: Residual deviation for not linear TTs and sample height for the LLP for the the residual method, Run 2 system, time slice n-1.

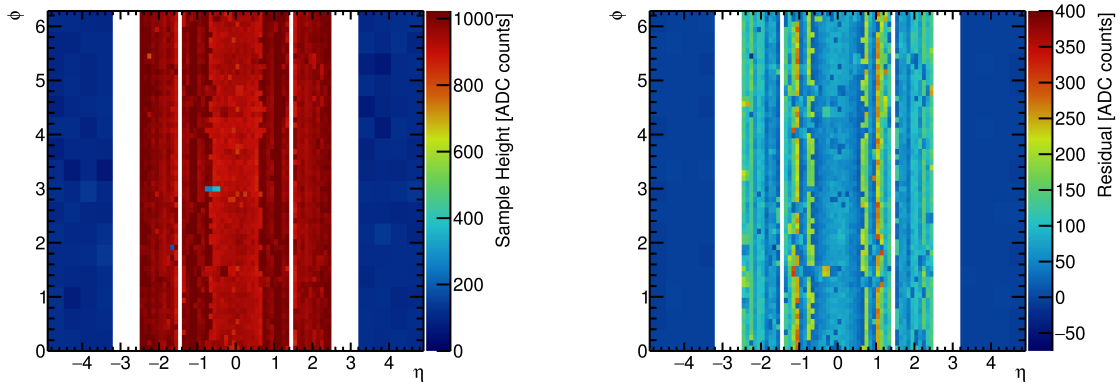

(a) Sample height NLP.

(b) Residual deviation NLP.

Figure B.4.: Sample height and residual deviation for the NLP for the χ^2_{red} threshold method, Run 2 system, time slice n-1.

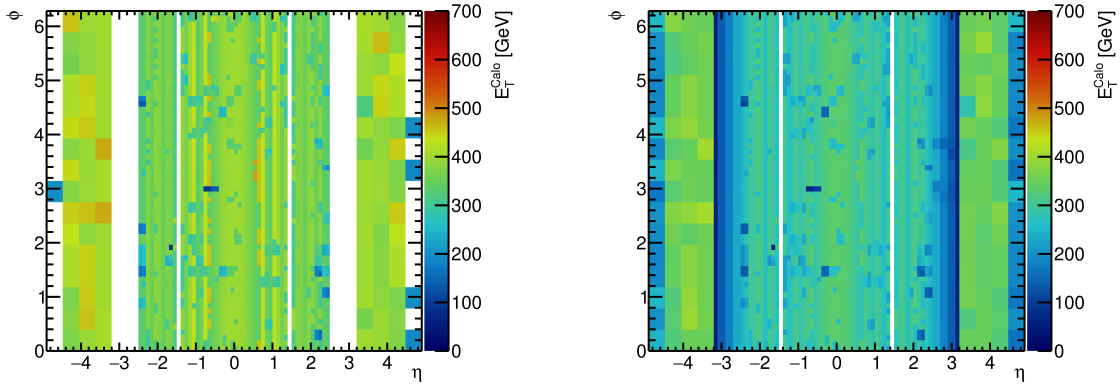

(a) $E_{\mathrm{T}}^{\mathrm{Calo}}$ NLP. (b) $E_{\mathrm{T}}^{\mathrm{Calo}}$ LLP.

Figure B.5.: $E_{\mathrm{T}}^{\mathrm{Calo}}$ values for the NLP and the LLP, Run 2 system, time slice n-1.

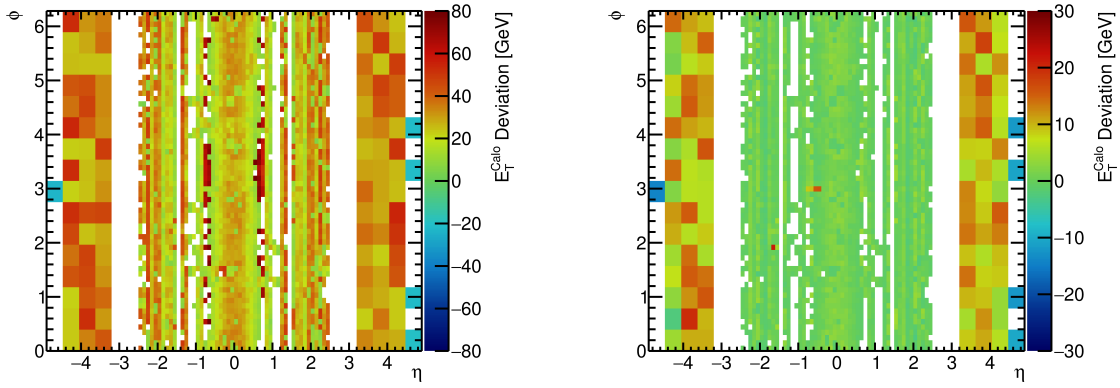

(a) $E_{\mathrm{T}}^{\mathrm{Calo}}$ deviation NLP for not linear TTs. (b) $E_{\mathrm{T}}^{\mathrm{Calo}}$ deviation LLP for not linear TTs.

Figure B.6.: $E_{\mathrm{T}}^{\mathrm{Calo}}$ deviation for the NLP and the LLP, Run 2 system, time slice n-1.

B.3. Time Slice n-2

Figure B.7a shows the residual deviation for the last linear point for all not linear TTs. The not linear FCal TT show residuals greater than 20 ADC counts after being included in the fit. This is due to the fit instability at low $E_{\mathrm{T}}^{\mathrm{Calo}}$. In Figure B.7b, the sample height for the last linear point is given. In the central region, the pulser runs do not exceed 300 ADC counts except for $(1.0 < |\eta| < 1.4)$ and $|\eta| = 2.4$, where up to 700 ADC counts are reached. The sample heights for linear but not saturated TTs are below 50 ADC counts in the EMEC inner wheel and FCal.

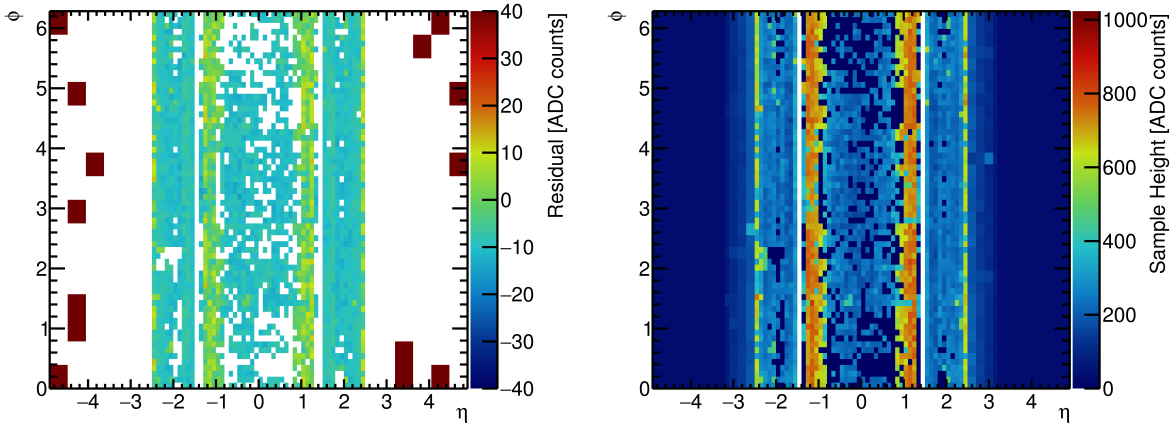

(a) Residual deviation LLP not linear TTs.

(b) Sample Height LLP.

Figure B.7.: Residual deviation for not linear TTs and sample height for the LLP for the residual method, Run 2 system, time slice n-2.

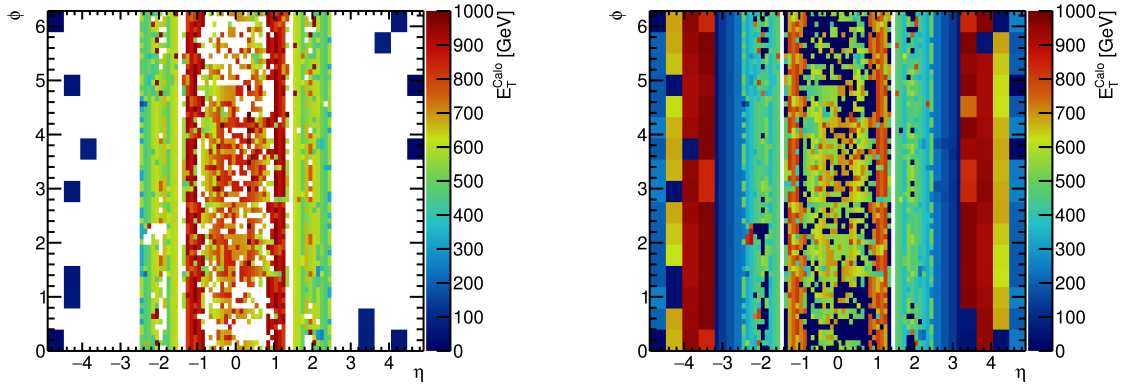

(a) $E_{\mathrm{T}}^{\mathrm{Calo}}$ NLP.

(b) $E_{\mathrm{T}}^{\mathrm{Calo}}$ LLP.

Figure B.8.: $E_{\mathrm{T}}^{\mathrm{Calo}}$ values for the NLP and LLP for the residual method, Run 2 system, time slice n-2.

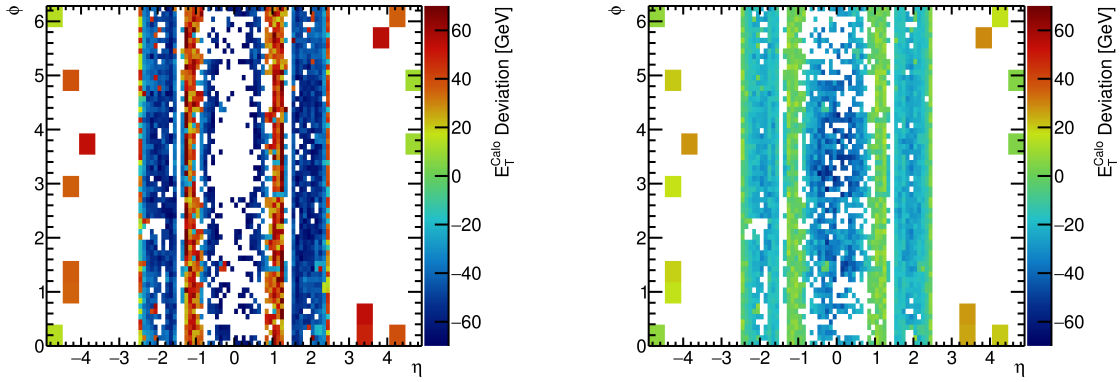

(a) $E_{\mathrm{T}}^{\mathrm{Calo}}$ deviation NLP for not linear TTs. (b) $E_{\mathrm{T}}^{\mathrm{Calo}}$ deviation LLP for not linear TTs.

Figure B.9.: $E_{\mathrm{T}}^{\mathrm{Calo}}$ deviation for the NLP and the LLP for not linear TT for the residual method, Run 2 system, time slice n-2.

B.4. Time Slices n-0.5, n-1.5

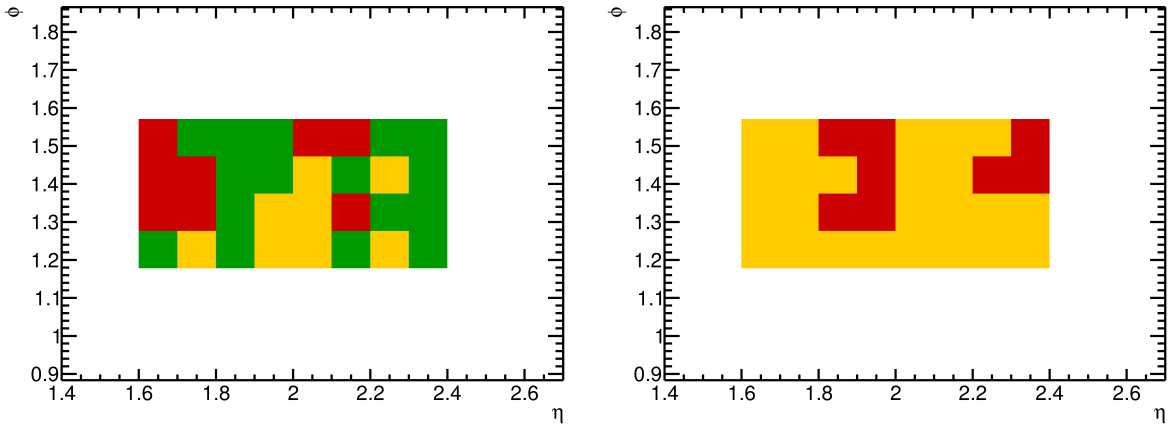

(a) Time slice n-0.5.

(b) Time slice n-1.5.

Figure B.10.: TT linearity characterisation for the new LTDB installed at the time of this thesis for time slices n-0.5 and n-1.5 for the residual method with residual threshold 20 ADC counts, time slice n. The Phase-I Upgrade signal latency is not corrected.
TT characterisation: linear until saturation – green, linear but not saturated – blue, not linear with $20 \leq |\text{residual}| \leq 30$ – orange, not linear with $|\text{residual}| > 30$ – red. All TTs are classified not linear.

Bibliography

[1] M. Aleksa, W. Cleland, Y. Enari, M. Fincke-Keeler, L. Hervas, F. Lanni, S. Majewski, C. Marino, and I. Wingerter-Seez et al. ATLAS Liquid Argon Calorimeter Phase-I Upgrade Technical Design Report. Technical Report CERN-LHCC-2013-017. ATLAS-TDR-022, CERN, September 2013. URL `http://cds.cern.ch/record/1602230`. Final version presented to December 2013 LHCC.

[2] Oliver Sim Brüning, Paul Collier, P Lebrun, Stephen Myers, Ranko Ostojic, John Poole, and Paul Proudlock. *LHC Design Report*. CERN Yellow Reports: Monographs. CERN, Geneva, 2004. doi: 10.5170/CERN-2004-003-V-1. URL `http://cds.cern.ch/record/782076`.

[3] ATLAS Collaboration. Luminosity determination in pp collisions at $\sqrt{s} = 13$ TeV using the ATLAS detector at the LHC. Technical Report ATLAS-CONF-2019-021, CERN, Geneva, June 2019. URL `http://cds.cern.ch/record/2677054`.

[4] The ATLAS Collaboration. The ATLAS experiment at the CERN Large Hadron Collider. *Journal of Instrumentation*, 3(08):S08003–S08003, August 2008. doi: 10.1088/1748-0221/3/08/s08003. URL `https://doi.org/10.1088%2F1748-0221%2F3%2F08%2Fs08003`.

[5] Frédérick Bordy Eckhard Elsen. A successful conclusion to Run 2. https://home.cern/news/opinion/accelerators/successful-conclusion-run-2, December 2018. Last accessed 25 July 2019.

[6] R. Achenbach et al. The ATLAS Level-1 Calorimeter Trigger. *Journal of Instrumentation*, 3(03):P03001–P03001, March 2008. doi: 10.1088/1748-0221/3/03/p03001. URL `https://doi.org/10.1088%2F1748-0221%2F3%2F03%2Fp03001`.

[7] Rene Brun et al. TProfile Class Reference, Root Version 6.19/01. https://root.cern.ch/doc/master/classTProfile.html.

[8] J. Jongmanns, M. Wessels, G. Andrei, F. Bartels, S. Franchino, M. Klassen, F. Napolitano, K. Schmitt, H.-C. Schultz-Coulon, T.M. Spieker, R. Stamen, S. M. Weber, and X. Yue et al. Performance of the upgraded PreProcessor of the ATLAS Level-1 Calorimeter Trigger (Unpublished). Technical Report ATL-COM-DAQ-2019-035, CERN, Geneva, February 2019. URL `https://cds.cern.ch/record/2661780`.

[9] CERN Press Office. CERN experiments observe particle consistent with long-sought Higgs boson. https://home.cern/news/press-release/cern/cern-experiments-observe-particle-consistent-long-sought-higgs-boson, July 2012. Last accessed 27 July 2019.

[10] Sebastian Weber. Studies and Improvements of the Bunch-crossing Identification for the ATLAS Level-1 Calorimeter Trigger. Master thesis, Universität Heidelberg, 2016.